

Hyperelastic stability landscape: A check for HILL stability of isotropic, incompressible hyperelasticity depending on material parameters

Herbert Baaser, University of Applied Sciences Bingen, Germany

December 3, 2025

Abstract

In this paper, we describe a uniform and standardized approach for analytically verifying the stability of isotropic, incompressible hyperelastic material models. Here, we address *stability* as fulfillment of the HILL condition – i.e. the positive definiteness of the material modulus in the KIRCHHOFF stress – log-strain relation. For incompressible material behavior, all mathematically and mechanically possible deformations lie within a range bounded, on the one hand, by uniaxial states and, on the other hand, by biaxial states; shear deformation states lie in between. This becomes particularly clear when the possible states are represented in the invariant plane. This very representation is now also used to visualize the regions of unstable material behavior depending on the selected strain energy function and the respective data set of material parameters. This demonstrates how, for some constellations of energy functions, with appropriate selection or calibration of parameters, stable and unstable regions can be observed. If such cases occur, it is no longer legitimate to use them to initiate, for example, finite element simulations. This is particularly striking when, for example, a fit appears stable in uniaxial tension, but the same parameter set for shear states results in unstable behavior without this being specifically investigated. The presented approach can reveal simple indicators for this. Nevertheless, the *simple shear* deformation, where the principal axes lag behind the deformation $\gamma = \tan \alpha$ of the shear angle α , i.e. the rotation tensor $\mathbf{R} \neq \mathbf{I}$, still represents a special case that requires extra investigations. This is especially true given that all shear components of the logarithmic strains themselves exhibit a non-monotonic behavior with respect to the deformation angle.

1 Introduction

The representation of classical isotropic hyperelasticity as a function of the input variables in the form of deformation invariants, see [17], or of the stretches themselves, see [33], is still of importance, especially when – as here – stability

statements of the models are concerned when used in the context of the finite element method (FEM). The special case of *quasi*-incompressibility is treated as a constraint within the framework of FEM, see modern textbooks such as [42] or more recent literature, but it is very well suited in this context to analytically describe the procedure and to identify specific properties of the models. In this context of material parameter calibration, we limit ourselves exclusively to ideal-incompressible deformation states. Elastomers in technical products for vibration control and sealing technology are frequently mentioned as a class of materials that exhibit almost ideal incompressibility.

This work can be read in series with [7] and [8], where "three natural strain invariants" $K_1 = \log J$ as "amount-of-dilatation", $K_2 = \|\operatorname{dev} \log \mathbf{v}\|$ as "magnitude-of-distortion" and $K_3 = \frac{3\sqrt{6}}{K_2} \det(\operatorname{dev}(\log \mathbf{v}))$ as "mode-of-distortion" are proposed based on the left polar decomposition of the deformation gradient $\mathbf{F} = \mathbf{v} \cdot \mathbf{R}$, see [32], with $J = \det \mathbf{F}$ in order to specify hyperelastic deformation modes alternatively. In that sense, one can distinguish the *prototype deformation modes* from each other by $K_3 = 0$ for pure shear, $K_3 = 1$ for uniaxial tension and $K_3 = -1$ for equibiaxial tension.

In a similar way, it was also possible in [5] to find a formulation that depends significantly only on the stretch in the tensile direction and is used here because this representation allows a further derivation of the stress in a simple way. Starting from the general representation of the standard invariants

$$\begin{aligned} I_1 &= \lambda_1^2 + \lambda_2^2 + \lambda_3^2, \\ I_2 &= \lambda_1^2 \lambda_2^2 + \lambda_1^2 \lambda_3^2 + \lambda_2^2 \lambda_3^2, \\ I_3 &= \lambda_1^2 \lambda_2^2 \lambda_3^2 =: J^2 \end{aligned} \quad (1)$$

as a function of the stretches $\lambda_{1,2,3}$ and its specification for the incompressible case with $J := \det \mathbf{F} \equiv 1$ and $\lambda_3 = (\lambda_1 \lambda_2)^{-1}$ as

$$\bar{I}_1 = \lambda_1^2 + \lambda_2^2 + \frac{1}{\lambda_1^2 \lambda_2^2} \quad \text{and} \quad \bar{I}_2 = \lambda_1^2 \lambda_2^2 + \frac{1}{\lambda_1^2} + \frac{1}{\lambda_2^2} \quad (2)$$

we directly obtain

$$\bar{I}_{1,m} = \lambda^2 + \lambda^{2m} + \lambda^{-2m-2} \quad \text{and} \quad \bar{I}_{2,m} = \lambda^{-2} + \lambda^{-2m} + \lambda^{2m+2} \quad (3)$$

as functions of an (uniaxial) stretch (intensity) λ and an additional parameter $m = [-\frac{1}{2} \dots 0 \dots 1]$ to specify the deformation mode *uniaxial tension* ($m = -\frac{1}{2}$), *pure shear* ($m = 0$, often called *plane strain*) and *equibiaxial tension* ($m = 1$), respectively. This ends up in the representation of the modes as boundary lines of all possible deformations in case of incompressibility in the *plane of invariants*, following e.g. [39]. In the Appendix A.2 we give more details on this graphical representation.

In [3] and recently in [18] based on [43], a very useful representation of the three squared stretches $\lambda_1^2, \lambda_2^2, \lambda_3^2$ as functions of the classical invariants I_1, I_2 is given for incompressible hyperelasticity in analytical form, i.e. $J = \lambda_1 \lambda_2 \lambda_3 \equiv 1$

or $I_3 = J^2 = 1$, equivalently. In addition, here we give an equivalent representation and conversion of any given incompressible deformation state $\lambda_1^2, \lambda_2^2, \lambda_3^2$ or \bar{I}_1, \bar{I}_2 into the (λ, m) representation given above, see Appendix A.1 for a short description and derivation of that closed form representation — to the knowledge of the author for the first time. In consequence, any given representation $\lambda_1^2, \lambda_2^2, \lambda_3^2$ with $\lambda_1 \lambda_2 \lambda_3 \equiv 1$ or \bar{I}_1, \bar{I}_2 can be converted into each other, in both directions, as needed. In this series there are also new investigations [23] on the stability specifically for the MOONEY–RIVLIN model, which is also used here, where, among other things, the relationship between the two material parameters of this model is investigated. There, stability in the three prototype deformation modes from above is defined as positive slope of the CAUCHY stress versus the relevant stretch λ , i.e. the CAUCHY stress–stretch curve must be monotone increasing.

Here, an analogue representation of isotropic hyperelasticity is given in a general form, in the sense that the three prototype deformations (uniaxial tension, shear and equibiaxial tension) are formulated uniformly based on (3). From this, a map of possible regions of material stability is developed, following the stability criteria in modern FEM codes such as ABAQUS or ANSYS, see [2]; the application of the HILL stability criterion¹ for general, incompressible hyperelastic models formulated as a potential function in \bar{I}_1 and \bar{I}_2 or equivalently in $\lambda_{1,2,3}$, as already given in [9] based on [14]. It must be mentioned that deformations with rotating principal axes, such as *simple shear*, are indeed included in the consideration of the plane of invariants (see [5]), but cases of non-monotone CAUCHY stress behavior can certainly be shown there, which will be discussed further, see [30], [41] and a simple example in Appendix E.

The aim of this work is to consistently apply these findings to verify the stability of the material formulation and to visualize it in a suitable mathematical–mechanical space. This leads to the graphical representation of the results in the *plane of invariants*, see [39], showing systematically the stability of material models based on their parameters. We consider a strictly one–dimensional stability marker $D_{1D}^m > 0$, generalizing the CAUCHY stress monotonicity from the three prototype modes to the whole plane of invariants and the full HILL’s inequality for the incompressible case. To this end, we derive a concise formulation of HILL’s inequality based on the positive definiteness of a projected HESSE matrix. These methods are both analytically and numerically verifiable and directly correspond to typical requirements in finite elements codes such as ABAQUS or ANSYS. The application of the formulation used here with tools for the automatic, analytical derivation of arbitrary energy potentials allows this graphical representation in, for example, MATLAB or EXCEL as a function of

¹In ABAQUS denoted vaguely as material stability or DRUCKER stability criterion with respect to the references given therein. The DRUCKER criterion is best known in *geometrically linearized elasticity* as $d\sigma : d\epsilon > 0 \iff \langle \sigma(\epsilon_1) - \sigma(\epsilon_2), \epsilon_1 - \epsilon_2 \rangle > 0 \quad \forall \epsilon_1 \neq \epsilon_2$ expressing the convexity of the strain energy in the infinitesimal strain $\epsilon = \frac{1}{2}[\nabla \mathbf{u} + (\nabla \mathbf{u})^T]$ as symmetrized gradient of the field of displacements $\mathbf{u} = [u_1 \ u_2 \ u_3]^T$ with $\nabla \mathbf{u} = \frac{\partial u_i}{\partial x_j}$ in three–dimensional space ($i, j = 1, 2, 3$). For linear isotropy, this DRUCKER criterion amounts to $\mu > 0, \kappa > 0$, where μ is the shear modulus, and κ is the bulk modulus.

the material parameters.

2 Background of stability analysis

We denote the first PIOLA–KIRCHHOFF stress tensor by \mathbf{S}_1 and $\mathbf{F} = \partial \mathbf{x} / \partial \mathbf{X}$ the deformation gradient between the actual configuration \mathbf{x} and the reference configuration \mathbf{X} . Thus, the mechanical power $\mathcal{P} = \mathbf{S}_1 : \dot{\mathbf{F}}$ results from the rate of the deformation gradient \mathbf{F} . Please note in this context the identity of the true CAUCHY stress $\boldsymbol{\sigma}$ and the KIRCHHOFF stress $\boldsymbol{\tau} = J\boldsymbol{\sigma} = \mathbf{S}_1 \cdot \mathbf{F}^T$ in the case of incompressibility, i.e. $J = \det \mathbf{F} \equiv 1$.

Our investigations follow recent works such as [10] and [13] developing [15], [38] and [16], where *the notion of conjugate pairs of stress and strain measures [...]* is introduced. Already RICHTER [34] uses a logarithmic strain matrix is used, in which the separation into volumetric and isochoric parts is realized by a deviatoric representation. Thus, following [35] the simplest definition of the strain tensor appears to be the logarithmic deformation matrix.

The fundamental recent investigation in [30] gives a theoretical underpinning of the natural appearance of the logarithmic strains based on the "corotational stability postulate" (CSP), i.e. for any reasonable corotational rate $\frac{D^\circ}{Dt}$ of the CAUCHY stress $\boldsymbol{\sigma}$ it applies

$$\left\langle \frac{D^\circ}{Dt} \boldsymbol{\sigma}, \mathbf{d} \right\rangle > 0 \quad \forall \mathbf{d} \neq \mathbf{0} \quad (4)$$

with $\mathbf{d} := \frac{1}{2}(\mathbf{l} + \mathbf{l}^T)$ as symmetric part of the spatial velocity gradient $\mathbf{l} := \text{grad } \dot{\mathbf{x}} = \dot{\mathbf{F}} \cdot \mathbf{F}^{-1}$. The ZAREMBA–JAUMANN rate $\frac{D^{ZJ}}{Dt}$ is one prototype corotational rate. It is further motivated, that *the corotational stability postulate (CSP) is a reasonable constitutive stability postulate in nonlinear elasticity, complementing local material stability viz. LEGENDRE–HADAMARD–ellipticity*. In the case of compressibility, not treated here, condition (4) is fully equivalent to

$$\begin{aligned} \mathbf{d}\boldsymbol{\sigma} : \mathbf{d}\boldsymbol{\epsilon}^{\log} &= \langle \mathbf{d}\boldsymbol{\sigma}, \mathbf{d}\boldsymbol{\epsilon}^{\log} \rangle \stackrel{!}{>} 0 \\ &= d\sigma_1 d\epsilon_1^{\log} + d\sigma_2 d\epsilon_2^{\log} + d\sigma_3 d\epsilon_3^{\log} > 0 \quad \forall \mathbf{v}_1 \neq \mathbf{v}_2 \iff \\ &\langle \boldsymbol{\sigma}(\log \mathbf{v}_2) - \boldsymbol{\sigma}(\log \mathbf{v}_1), \log(\mathbf{v}_2) - \log(\mathbf{v}_1) \rangle > 0 \quad \forall \mathbf{v}_1 \neq \mathbf{v}_2 \end{aligned} \quad (5)$$

and amounts to the fundamental *True–Stress–True–Strain Monotonicity* condition ("TSTS–M⁺") proposed for study of elastic stability in [29] and [30].

Given that and following [14, 15, 9, 38], "HILL stability" for the incompressible case can be expressed as

$$\mathbf{d}\boldsymbol{\sigma} : \mathbf{d}\boldsymbol{\epsilon}^{\log} = \langle \mathbf{d}\boldsymbol{\sigma}, \mathbf{d}\boldsymbol{\epsilon}^{\log} \rangle \stackrel{!}{>} 0, \quad \text{trace}(\mathbf{d}\boldsymbol{\epsilon}^{\log}) = 0 \iff \quad (6)$$

$$\langle \boldsymbol{\sigma}(\log \mathbf{v}_2) - \boldsymbol{\sigma}(\log \mathbf{v}_1), \log(\mathbf{v}_2) - \log(\mathbf{v}_1) \rangle > 0 \quad \forall \mathbf{v}_1 \neq \mathbf{v}_2, \det \mathbf{v}_1 = \det \mathbf{v}_2 = 1,$$

where $d\sigma$ denotes the increment of true CAUCHY stress², ϵ^{\log} the logarithmic HENCKY strain and ":" the double contracting tensor product, i.e. a scalar representation $s = A_{ij}B_{ij}$ for second order tensors \mathbf{A} and \mathbf{B} ; \mathbf{v}_1 and \mathbf{v}_2 with $\mathbf{v} = \mathbf{F} \cdot \mathbf{R}^{-1}$ denote any left stretch tensors, see also [41] recently.

Since $\tau = \sigma$ for incompressibility, that means, as in [15], HILL stability is more precisely associated with the statement

$$d\tau : d\epsilon^{\log} > 0, \quad \text{trace}(d\epsilon^{\log}) = 0 \iff (7)$$

$$\langle \tau(\log \mathbf{v}_2) - \tau(\log \mathbf{v}_1), \log(\mathbf{v}_2) - \log(\mathbf{v}_1) \rangle > 0 \quad \forall \mathbf{v}_1 \neq \mathbf{v}_2, \det \mathbf{v}_1 = \det \mathbf{v}_2 = 1,$$

which implies that the deviatoric part of the KIRCHHOFF stress τ is a monotone function of $\log \mathbf{v}$. The latter statement is the generic condition of HILL stability for compressible solids.

In modern FE-codes, the evaluation of (7) seems to be the crucial point to check or guarantee for material stability; in the sense of (6)₁ as given in ABAQUS User's Manual [2], Sec. 21.5.1, the check of stability is enforced for the three [here called "prototype"] deformation modes uniaxial tension, equibiaxial tension, planar tension, i.e. pure shear, performing it for the polynomial models, the OGDEN potential, the VAN DER WAALS form [...]. This check is executed only for each model once before the simulation is started individually in tension and compression direction, for $\lambda = 0.1$ up to $\lambda = 10$ by increments of $\Delta\lambda = 0.01$. In the ANSYS Mechanical APDL Theory Manual [4] [Section 4.6.9., eqn. (4.225)] the same statements are given concerning the MOONEY–RIVLIN, the OGDEN and the polynomial form hyperelastic material models, i.e. the check is performed for the Kirchhoff stress tensor corresponding to a change in the logarithmic strain.

In the Appendix A.2 we give the analytical derivation of the function $\bar{I}_2^{\text{uniax}} = \bar{I}_2^{\text{uniax}}(\bar{I}_1^{\text{uniax}})$ exemplary for the here given uniaxial deformation mode in blue, see Fig. 1. The corresponding boundary line for the biaxial deformation mode (here in red) is obtained in an analogous way and represents the reflection of the curve at the angle bisector, the green line of the shear deformation modes.

In addition, we remark that a biaxial deformation along x_1 and x_2 with $\lambda_{\text{biax}} > 1$ can be interpreted (and experimentally observed) as uniaxial compression with $\lambda_{\text{uniax}} < 1$ and vice versa, see Fig. 2 for illustration. Furthermore, in Fig. 3 we specify the relationship between "equivalent" mode parameters m and m^* . This equivalence describes the sign change from positive to negative m and vice versa. This can be seen as proof that the blue and red lines in Fig. 1 are each reflected across the (green) angle bisector. However, this does not mean that iso-lines for "m" are also reflected across the angle bisector. In the Appendix A.1 and the Appendix A.2 we give more details and further insights into possible derivations for these connections of m and m^* for $\lambda > 1$ and $\lambda < 1$.

²In former ABAQUS implementations (see [1]) the increments of the KIRCHHOFF stress $d\tau$ are used, whereas now (see [2]) the relation (8) seems to be used. In [29] it has been shown that (6) coincides with the corotational stability postulate (CSP) for incompressibility. Nonetheless, to the understanding of the author, ABAQUS and ANSYS use HILL's condition also in the compressible case as stability indicator. Then, HILL's condition is not equivalent to TSTS–M⁺ (5) and loses its physical significance.

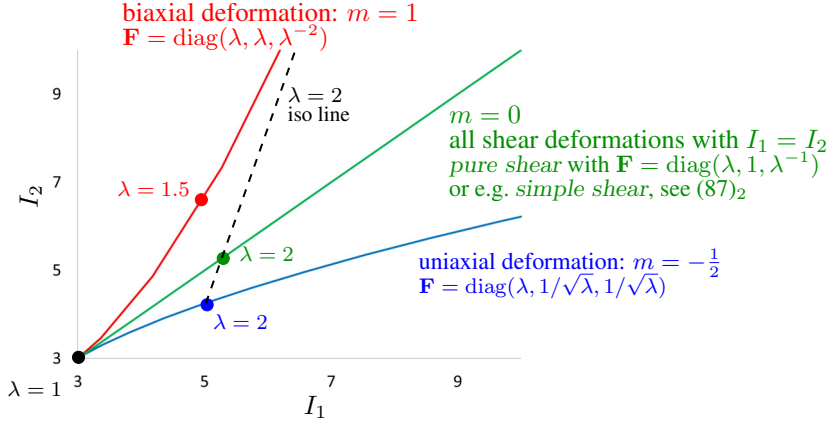


Figure 1: Illustration of ABAQUS check for stability only for the three special deformation modes in the plane of invariants up to $\lambda_* = 10$. In addition, we give the $\lambda = 2$ -iso line in that diagram exemplary for all $\lambda = \text{const}$ -iso lines as straight lines across that plane. Note that a proof is still pending that monotonicity of the KIRCHHOFF stress τ with respect to $\log \mathbf{v}$ in the three prototype deformation modes simultaneously implies monotonicity in all deformations without rotating principal axes, i.e. where \mathbf{F} is diagonal. However, HILL's condition (7) implies for all deformation modes without rotating principal axes, that the relevant stress curve must be monotone, see [30]. Here, we will only check the above monotonicity as a necessary condition for (6).

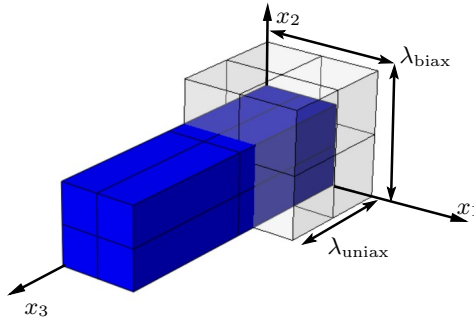


Figure 2: A biaxial deformation along x_1 and x_2 with $\lambda_{\text{biax}} > 1$ can be interpreted (and experimentally observed) as uniaxial compression in x_3 direction with $\lambda_3 = \lambda_{\text{uniax}} < 1$.

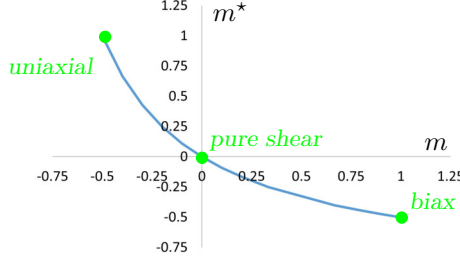


Figure 3: Equivalence of m and m^* in the sense of a change of sign in tension ($\lambda > 1$) and compression ($\lambda < 1$). Exemplary, $m = 1$ for the biaxial deformation mode corresponds to $m^* = -0.5$ as uniaxial mode, see Appendix A.2 and Fig. 14.

As denoted furtheron in ABAQUS User's Manual [2], Sec. 21.5.1, "the material is assumed to be incompressible, [and we] can choose any value for the hydrostatic pressure without affecting the strains. A convenient choice for the stability calculation is $\sigma_3 = d\sigma_3 = 0$." So, (6) is reformulated in the case of incompressible isotropy and in terms of the principal stresses and strains to

$$\begin{bmatrix} d\tau_1 \\ d\tau_2 \end{bmatrix} = \begin{bmatrix} d\sigma_1 \\ d\sigma_2 \end{bmatrix} = \underbrace{\begin{bmatrix} D_{11} & D_{12} \\ D_{21} & D_{22} \end{bmatrix}}_{=: \mathbb{D}} \cdot \begin{bmatrix} d\epsilon_1^{\log} \\ d\epsilon_2^{\log} \end{bmatrix} \quad (8)$$

with symmetric material stiffness tensor

$$\begin{aligned} \mathbb{D} &= \begin{bmatrix} D_{\log \lambda_1} \tau_1(\log \lambda_1, \log \lambda_2) & D_{\log \lambda_2} \tau_1(\log \lambda_1, \log \lambda_2) \\ D_{\log \lambda_1} \tau_2(\log \lambda_1, \log \lambda_2) & D_{\log \lambda_2} \tau_2(\log \lambda_1, \log \lambda_2) \end{bmatrix} \in \text{Sym}(2) \\ &= \begin{bmatrix} \lambda_1 D_{\lambda_1} \tau_1(\log \lambda_1, \log \lambda_2) & \lambda_2 D_{\lambda_2} \tau_1(\log \lambda_1, \log \lambda_2) \\ \lambda_1 D_{\lambda_1} \tau_2(\log \lambda_1, \log \lambda_2) & \lambda_2 D_{\lambda_2} \tau_2(\log \lambda_1, \log \lambda_2) \end{bmatrix} \end{aligned} \quad (9)$$

respecting for $\frac{d\lambda_i}{d \log \lambda_i} = \lambda_i$ for $i = 1, 2$, see (28) lateron. Alternative representations of \mathbb{D} are presented in the Appendix in (76) and (81). The stability is then checked by the positive definiteness of the tangent stiffness matrix \mathbb{D} with

$$\text{trace}(\mathbb{D}) = D_{11} + D_{22} > 0 \quad \text{and} \quad \det \mathbb{D} = D_{11} D_{22} - D_{12} D_{21} > 0, \quad (10)$$

see [2], whereas the classical conditions $D_{11} > 0$ and $\det \mathbb{D} > 0$ for positive definiteness of \mathbb{D} are indeed equivalent for symmetric 2×2 matrices. Summarizing, the built-in ABAQUS stability routine checks the positive definiteness of \mathbb{D} in (8) only along the uniaxial tension, the equibiaxial tension and the pure shear paths, see Fig. 1 and Fig. 11 in Section 3.2 below. Since the check of positive definiteness is given for a symmetric tensor \mathbb{D} , this shows that ABAQUS is really only considering HILL's inequality as mentioned in the footnote 2 before. For

that, in the Appendix B we give the MATLAB code for the evaluation of (8) exemplary for the YEOH example resulting in Fig. 11.

The evaluation of the principal stress components follows directly the representation of [17], p. 225 (6.69), given as

$$\sigma_a = -p + \lambda_a \left(\frac{dW}{d\bar{I}_1} \frac{d\bar{I}_1}{d\lambda_a} + \frac{dW}{d\bar{I}_2} \frac{d\bar{I}_2}{\lambda_2} \right) \quad (11)$$

for $a = 1, 2, 3$, whereas $\sigma_3 = \tau_3 = 0$ ("plane stress") from which we obtain

$$p = \lambda_3 \left(\frac{dW}{d\bar{I}_1} \frac{d\bar{I}_1}{d\lambda_3} + \frac{dW}{d\bar{I}_2} \frac{d\bar{I}_2}{\lambda_3} \right) \quad (12)$$

for the still open hydrostatic pressure component in (11). Reordering (11) and inserting p leads to

$$\begin{aligned} \tau_1 &= \sigma_1 = 2(\lambda^2 - \lambda^{-2m-2}) \frac{dW}{d\bar{I}_1} + 2(\lambda^{2m+2} - \lambda^{-2}) \frac{dW}{d\bar{I}_2}, \\ \tau_2 &= \sigma_2 = 2(\lambda^{2m} - \lambda^{-2m-2}) \frac{dW}{d\bar{I}_1} + 2(\lambda^{2m+2} - \lambda^{-2m}) \frac{dW}{d\bar{I}_2} \end{aligned} \quad (13)$$

in general for the two principal components at plane stress and incompressibility conditions, which now can be specified along the three paths of Fig. 1 leading each to

◊ $\lambda_1 = \lambda, \lambda_2 = \lambda_3 = \lambda^{-\frac{1}{2}}$ for *uniaxial tension* with $m = -\frac{1}{2}$,

$$\begin{aligned} \sigma_1 &= 2(\lambda^2 - \lambda^{-1}) \frac{dW}{d\bar{I}_1} + 2(\lambda - \lambda^{-2}) \frac{dW}{d\bar{I}_2}, \\ \sigma_2 &= 0 \end{aligned} \quad (14)$$

◊ $\lambda_1 = \lambda, \lambda_2 = 1, \lambda_3 = \lambda^{-1}$ for *pure shear* or *plane strain mode* with $m = 0$

$$\begin{aligned} \sigma_1 &= 2(\lambda^2 - \lambda^{-2}) \left(\frac{dW}{d\bar{I}_1} + \frac{dW}{d\bar{I}_2} \right), \\ \sigma_2 &= 2(1 - \lambda^{-2}) \frac{dW}{d\bar{I}_1} + 2(\lambda^2 - 1) \frac{dW}{d\bar{I}_2} \end{aligned} \quad (15)$$

◊ $\lambda_1 = \lambda_2 = \lambda, \lambda_3 = \lambda^{-2}$ for *biaxial tension* with $m = 1$, respectively,

$$\begin{aligned} \sigma_1 &= 2(\lambda^2 - \lambda^{-4}) \frac{dW}{d\bar{I}_1} + 2(\lambda^4 - \lambda^{-2}) \frac{dW}{d\bar{I}_2}, \\ \sigma_2 &= 2(\lambda^2 - \lambda^{-4}) \frac{dW}{d\bar{I}_1} + 2(\lambda^4 - \lambda^{-2}) \frac{dW}{d\bar{I}_2} = \sigma_1 \end{aligned} \quad (16)$$

in equivalence to [2].

In addition, we give the resulting principal stresses (13) exemplary for an arbitrary value of the mode parameter m , here e.g. $m = \frac{1}{3}$ as depicted lateron in Fig. 6:

$$\begin{aligned}\sigma_1 &= 2(\lambda^2 - \lambda^{-\frac{8}{3}}) \frac{dW}{d\bar{I}_1} + 2(\lambda^{\frac{8}{3}} - \lambda^{-2}) \frac{dW}{d\bar{I}_2}, \\ \sigma_2 &= 2(\lambda^{\frac{2}{3}} - \lambda^{-\frac{8}{3}}) \frac{dW}{d\bar{I}_1} + 2(\lambda^{\frac{8}{3}} - \lambda^{-\frac{2}{3}}) \frac{dW}{d\bar{I}_2}.\end{aligned}\quad (17)$$

Please note, for a concrete implementation of such a test procedure in a biaxial test rig [37], for example, on a thin rubber sample as depicted in Fig. 4, one can now specify the stretches in the form of displacement boundary conditions for the path of any m . The corresponding stresses then arise and can be measured

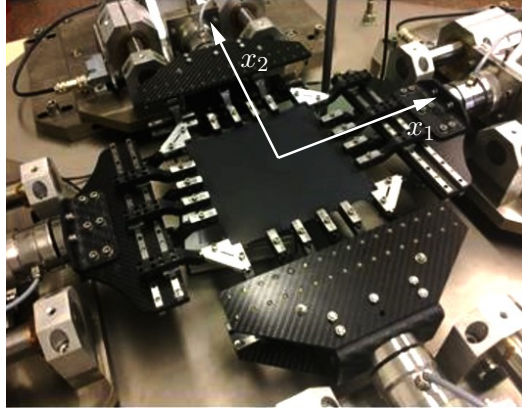


Figure 4: Possible experimental setup by a "biax-tester" from [37], where in the thickness direction x_3 an uniaxial compression now takes place, see Fig. 2.

as force quantities. This allows predictions from the different material models in the form of energy functions W to be compared with regard to their quality of the stress response in this test procedure.

2.1 Aspects of HILL's inequality

2.1.1 The compressible case

For a better understanding of the elastic stability concept considered here, it will be useful to summarize the properties of HILL's condition. Originally proposed by [14, 15] in the sense of a rate-condition for compressible response

$$\left\langle \frac{D^{ZJ}}{Dt} \boldsymbol{\tau}, \mathbf{d} \right\rangle > 0 \quad \forall \mathbf{d} \neq \mathbf{0}, \quad (18)$$

it can be shown to be equivalent to the following statements [29]:

$$\begin{aligned} &\iff \frac{d\boldsymbol{\tau}}{d \log \mathbf{v}} \text{ is a positive definite fourth order tensor} \\ &\iff \frac{d\boldsymbol{\tau}^i(\log \lambda_1, \log \lambda_2, \log \lambda_3)}{d \log \lambda_j} \text{ is a positive definite symmetric matrix} \\ &\iff W = \widehat{W}(\log \mathbf{v}) \text{ is convex in } \log \mathbf{v} \\ &\iff W = \widehat{W}(\log \lambda_1, \log \lambda_2, \log \lambda_3) \text{ is convex in } (\log \lambda_1, \log \lambda_2, \log \lambda_3) \\ &\iff \left\langle \underbrace{D^2 \widehat{W}(x_1, x_2, x_3)}_{=: \mathbb{H}} \cdot \boldsymbol{\eta}, \boldsymbol{\eta} \right\rangle_{\mathbb{R}^3} > 0 \quad \forall \boldsymbol{\eta} \neq \mathbf{0} \in \mathbb{R}^3 \\ &\iff \mathbb{H} \in \text{Sym}^{++}(3) : \text{trace}(\mathbb{H}) > 0, \text{trace}(\text{Cof } \mathbb{H}) > 0, \det \mathbb{H} > 0 \\ &\iff \langle \boldsymbol{\tau}(\log \mathbf{v}_1) - \boldsymbol{\tau}(\log \mathbf{v}_2), \log \mathbf{v}_1 - \log \mathbf{v}_2 \rangle > 0 \quad \forall \mathbf{v}_1 \neq \mathbf{v}_2 \\ &\iff \sum_{i=1}^3 (\boldsymbol{\tau}_i(\log \bar{\lambda}_1, \log \bar{\lambda}_2, \log \bar{\lambda}_3) - \boldsymbol{\tau}_i(\log \lambda_1, \log \lambda_2, \log \lambda_3)) (\log \bar{\lambda}_i - \log \lambda_i) > 0 \\ &\iff d\boldsymbol{\tau} : d\boldsymbol{\epsilon}^{\log} = d\tau_1 d\epsilon_1^{\log} + d\tau_2 d\epsilon_2^{\log} + d\tau_3 d\epsilon_3^{\log} > 0. \end{aligned} \quad (19)$$

2.1.2 The incompressible case

In the incompressible case HILL's inequality is evaluated for $\det \mathbf{F} = 1$. Since

$$\log \det \mathbf{F} = \log \det \mathbf{v} = \text{trace}(\log \mathbf{v}), \quad (20)$$

the nonlinear and non-convex constraint $\det \mathbf{F} = 1$ translates with respect to the logarithmic strains $\log \mathbf{v}$ into the linear and convex constraint

$$0 = \text{trace}(\log \mathbf{v}) = \log \lambda_1 + \log \lambda_2 + \log \lambda_3. \quad (21)$$

Therefore, we have

$$\begin{aligned}
&\iff \left\langle \frac{D^{ZJ}}{Dt} \boldsymbol{\tau}, \mathbf{d} \right\rangle > 0 \quad \forall \mathbf{d} \neq \mathbf{0}, \operatorname{trace}(\mathbf{d}) = 0 \\
&\iff W = \widehat{W}(\log \mathbf{v}) \quad \text{is convex in } \log \mathbf{v} \text{ over } \operatorname{trace}(\log \mathbf{v}) = 0 \\
&\iff W = \widehat{W}(\log \lambda_1, \log \lambda_2, \log \lambda_3) \quad \text{is convex in} \\
&\quad (\log \lambda_1, \log \lambda_2, \log \lambda_3) \text{ over } \log \lambda_1 + \log \lambda_2 + \log \lambda_3 = 0 \\
&\iff d\boldsymbol{\tau} : d\boldsymbol{\epsilon}^{\log} > 0 \text{ with } \operatorname{trace}(d\boldsymbol{\epsilon}^{\log}) = 0 \\
&\iff d\tau_1 d\epsilon_1^{\log} + d\tau_2 d\epsilon_2^{\log} + d\tau_3 d\epsilon_3^{\log} > 0 \quad \text{with } d\epsilon_1^{\log} + d\epsilon_2^{\log} + d\epsilon_3^{\log} = 0 \\
&\iff \left\langle \underbrace{D^2 \widehat{W}(x_1, x_2, x_3)}_{=: \mathbb{H}} \cdot \boldsymbol{\eta}, \boldsymbol{\eta} \right\rangle_{\mathbb{R}^3} > 0 \quad \forall \boldsymbol{\eta} \neq \mathbf{0}, \eta_1 + \eta_2 + \eta_3 = 0 \\
&\iff \left\langle \underbrace{\mathbf{P}^T \cdot D^2 \widehat{W}(x_1, x_2, x_3) \cdot \mathbf{P}}_{=: \mathbb{H}^{\text{inc}}} \cdot \boldsymbol{\xi}, \boldsymbol{\xi} \right\rangle_{\mathbb{R}^2} > 0 \quad \forall \boldsymbol{\xi} \in \mathbb{R}^2 \quad \text{with } \mathbf{P} = \begin{bmatrix} 0 & 1 \\ -1 & -1 \\ 1 & 0 \end{bmatrix} \\
&\iff \mathbb{H}^{\text{inc}} \in \operatorname{Sym}^{++}(2) : \operatorname{trace}(\mathbb{H}^{\text{inc}}) > 0, \det \mathbb{H}^{\text{inc}} > 0 \\
&\iff \text{the ABAQUS check: } \mathbb{D} \text{ from (8) is positive definite,} \tag{22}
\end{aligned}$$

where we show the last equivalence in Appendix D.3.

An evaluation of HILL's condition in rate-form (18) along the family

$$\mathbf{F} = \operatorname{diag}(\lambda, \lambda^m, \lambda^{-(m+1)}) \tag{23}$$

of the special, i.e. "prototype" deformations in Fig. 1 is given in the Appendix C. A numerical check of HILL's condition for compressibility and a family of elastic energies has recently been given in [12].

3 Derivations and further treatment: the uniaxial case as motivation

The aim of this contribution is a generalized procedure of evaluating (7) for given W in the *plane of invariants*, see [39] and [5], as a map of admissible and inadmissible regions for a set of material parameter c_1, c_2, c_3, \dots , on which the hyperelastic material description in terms of the elastic energy W depends.

As already known, see [17], and executed exemplary in e.g. [2], we obtain the stress response (11) in principal directions and derive here the stability check for the uniaxial case (14).

Let us describe the (incremental) stress-strain relationship $d\boldsymbol{\sigma} = \mathbb{D} : d\boldsymbol{\epsilon}^{\log}$ equivalent to (8) with $d\boldsymbol{\epsilon}^{\log}$ as increment in the HENCKY strain as in (6), i.e. the logarithmic strain $\boldsymbol{\epsilon}^{\log} = \operatorname{diag}(\log \lambda_1, \log \lambda_2, \log \lambda_3)$ by the stretches $\lambda_{1,2,3}$ in principal axes as the main diagonal of a $[3 \times 3]$ tensor/matrix notation, and the fourth order material modulus \mathbb{D} . In the one-dimensional uniaxial case, the

constitutive relation reduces to

$$d\sigma = D_{1D} d \log \lambda \quad (24)$$

with $\sigma(\lambda_1, \lambda_2) = \hat{\sigma}(\log \lambda_1, \log \lambda_2) = \hat{\sigma}(\lambda, m) = \tau$ for $J = 1$, which we refer to in this work. Following [34] and [41] recently, the KIRCHHOFF stress τ is conjugate to the logarithmic strain in the sense that

$$\tau = \frac{dW(\log \mathbf{v})}{d \log \mathbf{v}}, \quad (25)$$

which is reduced to the one-dimensional case (14) considered here. Exemplary,

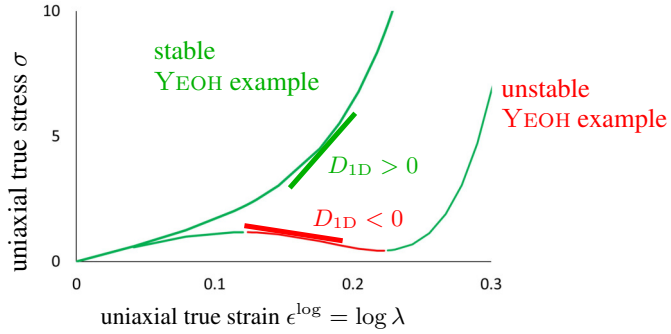


Figure 5: Example of uniaxial true stress–strain behaviour $\sigma(\log \lambda)$ for the YEOH model (31). In green a stable and monotone result using the parameters $c_1 = 1.0$ MPa, $c_2 = 0.1$ MPa and $c_3 = 0.3$ MPa; in red an unstable and non-monotonic result using the parameters $c_1 = 1.0$ MPa, $c_2 = -0.9$ MPa and $c_3 = 0.3$ MPa as used below in Tab. 1. The green and the red tangents symbolize the slope D_{1D} of the curves, which is given in (30) below.

we give an uniaxial stress–strain function according to the YEOH model used later on (31) in order to show D_{1D} of (24) and (26)₁.

We formulate according to [2]

$$D_{1D} = \frac{d\sigma}{d\epsilon^{\log}} = \frac{d\sigma}{d\lambda} \frac{d\lambda}{d\epsilon^{\log}} = \lambda \frac{d\sigma}{d\lambda}, \quad (26)$$

if we consider the derivative of the natural logarithm

$$\frac{d\epsilon^{\log}}{d\lambda} = \frac{d \log \lambda}{d\lambda} = \frac{1}{\lambda}, \quad (27)$$

and their reversal

$$\frac{d\lambda}{d \log \lambda} = \lambda \quad (28)$$

directly plugged in into (26)₂.

For further investigations we only use (26)₃ and check the expression for monotonicity, here $D_{1D} > 0$ for a given function W , whose stability now depends on the set of material parameters c_i for any deformation given by \bar{I}_1 and \bar{I}_2 or λ and m . Again, with that formulation (26)₃ enforcing (3), now we are able to come with the representation of the derivatives by

$$\tau = \sigma = \lambda \frac{dW}{d\lambda} \quad (29)$$

as already given by (14). Using (29) to evaluate directly and uniformly for the uniaxial case

$$\begin{aligned} D_{1D} = \lambda \frac{d\sigma}{d\lambda} &= 4c_1(\lambda^2 + \lambda^{-1}) + 8c_2(2\lambda^4 - 3\lambda^2 + \lambda - 3\lambda^{-1} + 3\lambda^{-2}) \\ &+ 12c_3(3\lambda^6 - 12\lambda^4 + 5\lambda^3 + 9\lambda^2 - 6\lambda + 2 + 9\lambda^{-1} - 18\lambda^{-2} + 8\lambda^{-3}) \end{aligned} \quad (30)$$

via (26)₃, we check the material stability by $D_{1D} \stackrel{?}{>} 0$ according to (6) and (7), respectively, and give that example in anticipation of the later used YEOH model (31).

Please note that the evaluation of (30) includes the consideration of the derivative with respect to $\log \lambda$ as in (28); and the insertion of the derivative of W_{Yeoh} as the potential for the stresses, which again results in this compact form. For the general form, see the next section – also using the MATLAB SYMBOLIC TOOLBOX [25]. This settles the question for the uniaxial case.

The case for general $m = (-\frac{1}{2} \dots 0 \dots 1)$ will be shown in the Appendix. Remember that $D_{1D} > 0$ is (only) necessary for HILL's inequality (7) to hold [30] and Appendix. The critical advantage of checking the scalar $D_{1D} > 0$ is its simplicity compared to checking \mathbb{D} from (8) for positive definiteness. And, in contrast to the ABAQUS procedure, the check can be easily performed along the whole plane of invariants.

3.1 Application of MATLAB SYMBOLIC TOOLBOX and stability map

We consider here as a first material model the strain energy (density) function according to YEOH [44] depending only on \bar{I}_1

$$W_{\text{Yeoh}} = c_1(\bar{I}_1 - 3) + c_2(\bar{I}_1 - 3)^2 + c_3(\bar{I}_1 - 3)^3 \quad (31)$$

with three parameters c_1, c_2, c_3 , which is known to possibly satisfy HILL's inequality (6) for incompressibility even for negative parameter c_2 depending on $c_{1,3} > 0$.

Knowing that automatic code generation for mathematical–mechanical implementations has reached a very high level as a result of [22] even based on the newest versions of MATHEMATICA [40], we use here, as recently in [11], the SYMBOLIC TOOLBOX of MATLAB [25] for the implementation of (31), (33), (34) and (38), (29) respectively, and the derivative in (26)₃. The MATLAB code example given here is realized for the MOONEY–RIVLIN strain energy function (33) in order to show a general case using both invariants \bar{I}_1 and \bar{I}_2

```

clear all
syms lam m I1 I2 c1 c2

% Mooney-Rivlin
W_MoRi = c1*(I1-3) + c2*(I2-3)

dW_dI1 = diff(W_MoRi,I1);
dW_dI2 = diff(W_MoRi,I2);

%
I1 = lam^2+lam^(2*m) + lam^(-2*(m+1))
dW_dI1 = subs(dW_dI1,I1, lam^2+lam^(2*m) + lam^(-2*(m+1)))
%
I2 = lam^(-2)+lam^(-2*m) + lam^(2*(m+1))
dW_dI2 = subs(dW_dI2,I2, lam^(-2)+lam^(-2*m) + lam^(2*(m+1)))

sig1 = 2*(lam^2-lam^(-2*m-2))*dW_dI1 ...
       + 2*(lam^(2*m+2)-lam^(-2))*dW_dI2
sig1 = collect(sig1,["c1" "c2" "c3"])

sig2 = 2*(lam^(2*m)-lam^(-2*m-2))*dW_dI1 ...
       + 2*(lam^(2*m+2)-lam^(-2*m))*dW_dI2
sig2 = collect(sig2,["c1" "c2" "c3"])

D_1D_m = diff(sig1, lam)+m*diff(sig2, lam)
D_1D_m = collect(D_1D_m,["c1" "c2" "c3"])

```

Here, $D_{1D,m}$ is now the complete and analytical representation of (26), derived from any strain energy function W . Given \bar{I}_1 and \bar{I}_2 for any stretch λ and mode exponent m , we represent $D_{1D,m}$, or (26) respectively, in visualizations as Fig. 6 – Fig. 10. Here, we give the more general derivation of D_{1D} and $\tau_3 = 0$ is incorporated in terms of

$$D_{1D}^m = D_\lambda \widehat{\tau}_1(\lambda) + m D_\lambda \widehat{\tau}_2(\lambda), \quad (32)$$

see (60) in the Appendix C, where we use the derivatives $D_\lambda \tau_1$ and $D_\lambda \tau_2$ of the principal stress components (13) obtained by the help of the MATLAB SYMBOLIC TOOLBOX [25], shown in the last two lines of the code example above.

Table 1: Exemplary material parameters for the YEOH model in MPa = $\frac{N}{mm^2}$.

c_1	c_2	c_3
1.0	-0.9	0.3

Such visualization in the form of a stability map in the plane of invariants enables a rapid identification of unstable parameter ranges and thus provides a tool for targeted parameter adjustment during material calibration. Thus, we

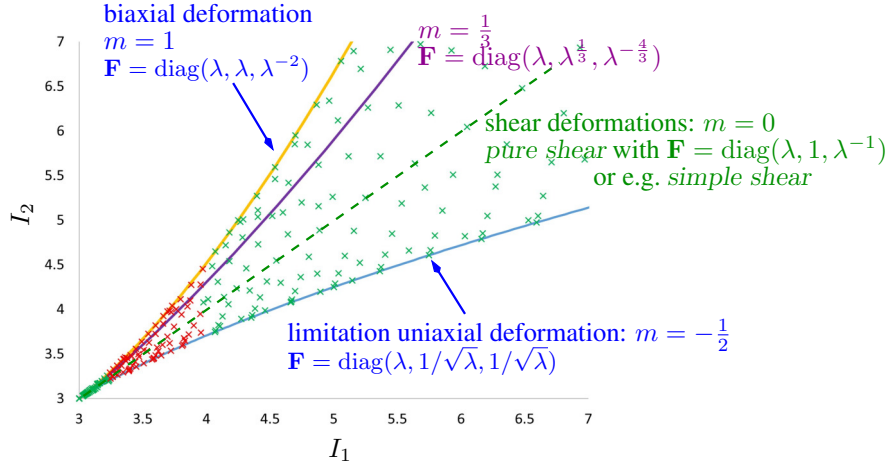


Figure 6: Plane of invariants as scope for visualization the material stability of the YEOH model: The **red** crosses here mark the instable region depending on the parameters in Tab. 1 according to the criterion $D_{1D}^m > 0$ of (32). In addition, the limiting lines of all possible states given by uniaxial and biaxial deformations are shown. All shear deformation states with $\bar{I}_1 \equiv \bar{I}_2$ exactly form the angle bisector of the diagram. The **magenta** line visualizes a path for $m = \frac{1}{3}$ in that plane exemplary. The density of the points is – here and in the following figures – a direct result of the incrementation of λ_* in steps of $\Delta\lambda_* = 0.1$ based on the choosen step size for the stability investigation in ABAQUS and ANSYS.

are now able to show by the proposed procedure visualized in a "heat" map, where **green** indicates the possibly stable region, whereas **red** the instable zone due to the parameter declaration for given deformations. Please note, that any shear deformation states (both *plane strain*, i.e. *pure shear*, with principal axes are fixed and *simple shear* with rotating principal axes) with $\bar{I}_1 = \bar{I}_2$ exactly form the angle bisector of the diagram. In this first exemplary case with parameters from Tab. 1, a picture emerges as in Fig. 6, where we provoked the instability by the negative parameter $c_2 < 0$. Here, it is clear that after an initially stable range near to the stress free origin, i.e. $\bar{I}_1 = \bar{I}_2 = 3$, the material behavior becomes unstable across the range of all possible deformations, see red crosses. Using the procedure presented here, it is now very easy to adjust, for example, the parameter c_2 to eliminate instability. Of course, the resulting adjustment must also be consistent with the experimental procedures performed on the material or components.

As a further example, we demonstrate the application to the incompressible MOONEY-RIVLIN model [36], known as the simplest model with I_1 and I_2 dependence:

$$W_{\text{MoRi}} = c_1 (I_1 - 3) + c_2 (I_2 - 3). \quad (33)$$

This model is known for its supposedly good fit to uniaxial tension experiments.

Firstly, we show the results of our approach for positive parameters as given in Tab. 2, which satisfy HILL’s condition everywhere and consistently yield a picture of stable results as in Fig. 7.

Table 2: Exemplary material parameters for the MOONEY–RIVLIN model in $\text{MPa} = \frac{\text{N}}{\text{mm}^2}$.

c_1	c_2
0.8	+0.6

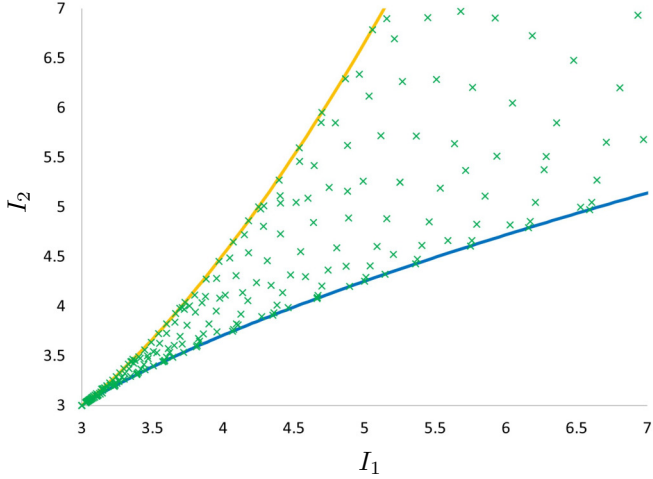


Figure 7: Plane of invariants as scope for visualization of the material stability of the MOONEY–RIVLIN model according to the criterion $D_{1D}^m > 0$: The green crosses mark the completely stable region depending on the parameters in Tab. 2.

Secondly, one can show a counterexample here: unfortunately, this ignores the fact that such a fit, here with negative parameter c_2 , can lead to unstable behavior in regions of shear and biaxial tension. This is highlighted again by the red markers in Fig. 8. Such parameter combinations often lead to non-

Table 3: Exemplary material parameters for the MOONEY–RIVLIN model in $\text{MPa} = \frac{\text{N}}{\text{mm}^2}$.

c_1	c_2
0.8	-0.2

convergent or unrealistic behavior in FEM simulations and should therefore be excluded in advance by stability analysis, i.e. even though a supposedly good fit

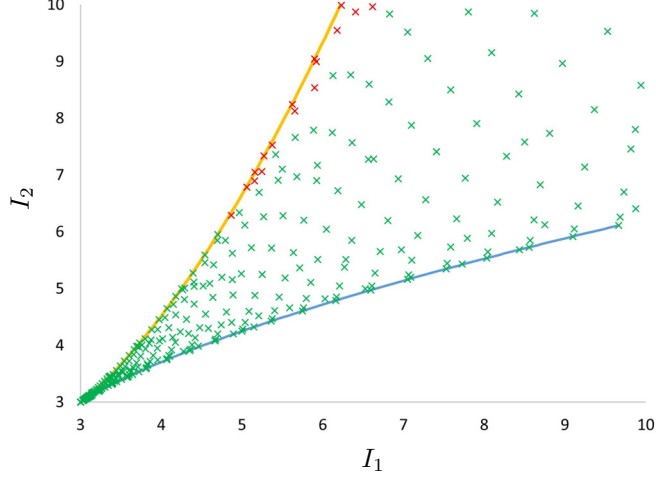


Figure 8: Plane of invariants as scope for visualization the material stability of the MOONEY–RIVLIN model: The red crosses here mark the unstable region depending on the parameters in Tab. 3 according to the criterion $D_{1D}^m > 0$ of (32): $c_1 = 0.8$ MPa and $c_2 = -0.2$ MPa

was achieved in the uniaxial tension. In Appendix D we reconsider W_{MoRi} (33) in order to have a more detailed look into stability statements incorporating the two invariants I_1 and I_2 .

As a next example, we describe a somewhat more complicated case, in that the derivation of this procedure is applied to the OGDEN model(s) [33], i.e. a formulation in the stretches and not directly in the invariants, as described in detail in [18] for special cases: Here, we consider exemplary the case of a 2nd order model

$$W_{\text{Ogden}} = \frac{2\mu_1}{\alpha_1^2}(\lambda_1^{\alpha_1} + \lambda_2^{\alpha_1} + \lambda_3^{\alpha_1} - 3) + \frac{2\mu_2}{\alpha_2^2}(\lambda_1^{\alpha_2} + \lambda_2^{\alpha_2} + \lambda_3^{\alpha_2} - 3) \quad (34)$$

with fixed $\alpha_1 := 6$ and $\alpha_2 := -4$, which is then equivalent to

$$W_{\text{Ogden}} = \frac{\mu_1}{18}(\bar{I}_1^3 - 3\bar{I}_1\bar{I}_2) + \frac{\mu_2}{8}(\bar{I}_2^2 - 2\bar{I}_1 - 3), \quad (35)$$

following [18] as advanced combination of (2.10)₂ and (2.12)₂ therein. Further combinations of this model class are discussed in [18]; a generalization using the closed-form conversion of a deformation state in the form of the stretches into the invariants given there, is still pending for the application in this work, see Appendix A.1, without diminishing the achievements presented here. However, this example, as before, shows that a supposedly good fit to uniaxial tension data causes unstable behavior in other deformation modes. This must be avoided in simulations.

Table 4: Exemplary material parameters for the OGDEN model in MPa = $\frac{\text{N}}{\text{mm}^2}$.

μ_1	μ_2
0.3	-0.2

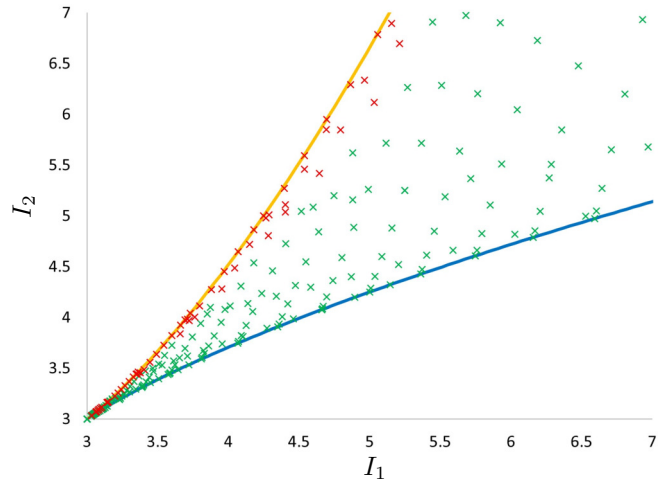


Figure 9: Plane of invariants as scope for visualization the material stability of the OGDEN model: The red crosses here mark the unstable region depending on the parameters in Tab. 4 according to the criterion $D_{1D}^m > 0$ of (32): $\mu_1 = 0.3$ MPa and $\mu_2 = -0.2$ MPa.

As a final and more extensive example, we apply the stability analysis procedure presented here to the *quadratic HENCKY model* proposed in [27], which is given by

$$W_{\text{Hencky}} = \mu \|\log \mathbf{v}\|^2 + \frac{\kappa}{2} \text{tr}^2(\log \mathbf{v}) \quad (36)$$

with $\mu > 0$ as shear modulus and $\kappa > 0$ as bulk modulus and $\text{tr}(\cdot)$ as matrix trace operator. Please note that this model in the *quadratic* form with "log \mathbf{v} " as strain tensor is not yet available in e.g. ABAQUS or other commercial FE-codes.

In the incompressible case with $\lambda_3 = (\lambda_1 \lambda_2)^{-1}$ this model (36) reduces to

$$W_{\text{Hencky}} = 2\mu (\log^2 \lambda_1 + \log^2 \lambda_2 + \log \lambda_1 \log \lambda_2). \quad (37)$$

Applying here the same arguments for the prototype deformations as in (3) from above, (37) is directly reformulated into

$$W_{\text{Hencky}} = 2\mu \left(\frac{2+m}{\lambda} \log \lambda + \frac{2m+1}{\lambda} \log(\lambda^m) \right) \quad (38)$$

in terms of the *stretch intensity* λ and the *mode parameter* m . The stress computation (13) allows us to reuse (38) directly in (26), which results in Fig. 10 for $\mu = 1$ MPa showing just stable situations in the plane of invariants.

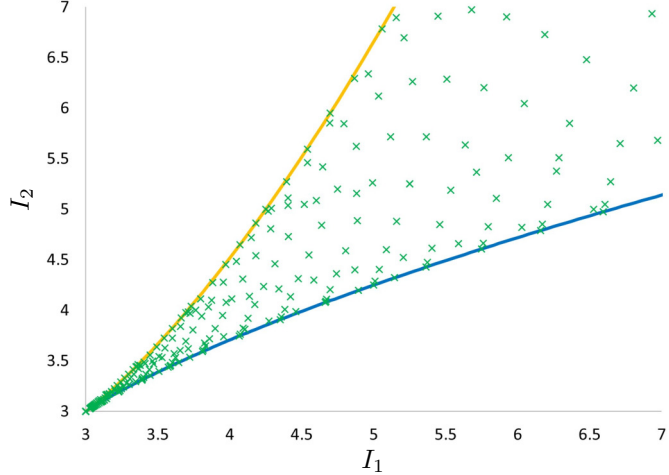


Figure 10: Plane of invariants as scope for visualization the material stability of the *quadratic HENCKY model* with material parameter $\mu > 0$ according to the criterion $D_{1D}^m > 0$ of (32): The green crosses here mark the complete stable region.

Since $\boldsymbol{\tau} = \frac{dW_{\text{Hencky}}}{d \log \mathbf{v}} = 2\mu \log \mathbf{v}$ we see $\boldsymbol{\tau}$ to clearly satisfy the HILL monotonicity condition (7). However, the shear stress component $\tau_{12} = 2\mu (\log \mathbf{v})_{12}$ with $\log \mathbf{v} = \frac{1}{2} \log \mathbf{b}$ is non-monotone in γ , as we show in the Appendix E. Again

we see that cases with rotating principal axes are not detected as unstable by the procedure above and additional criteria must be applied as suggested in [41] and [29]: namely to additionally require for stability the "LH-ellipticity" of the constitutive law.

In contrast, a nonlinear extension of the model (36) is the exponentiated HENCKY model

$$W_{\text{expH}} = \mu \exp(\|\log \mathbf{v}\|^2) + \frac{\lambda}{2} \exp((\log \det \mathbf{F})^2) \quad (39)$$

see [28] and [26] for a FE implementation. This model shows a monotonic behavior in the 12-true-shear-stress components.

3.2 Comparison with the ABAQUS stability check of $\mathbb{D} \in \text{Sym}^{++}(2)$

We refer to Section 2, where we discuss in detail the basic approach of the stability check of ABAQUS as presented in [2], section "Hyperelastic behavior of rubberlike materials", and present our extension to the entire plane of invariants. This figure (Fig. 11) should be compared to Fig. 6 showing the material

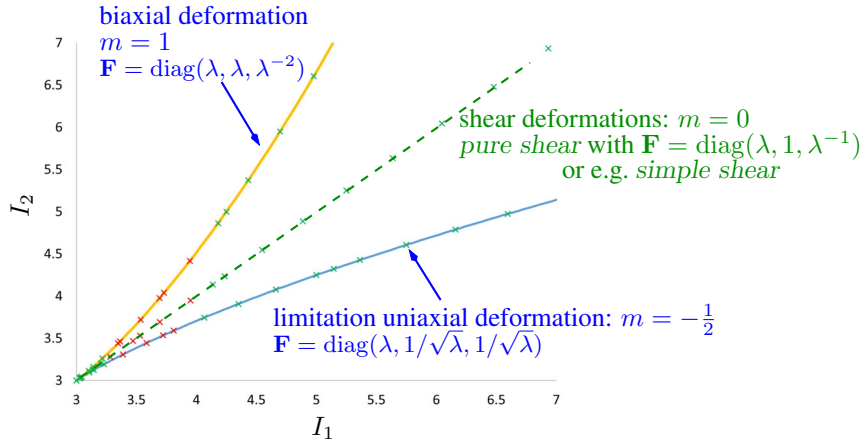


Figure 11: Plane of invariants as scope for visualization of the ABAQUS stability check for the YEOH model with the parameters in Tab. 1.

stability situation for the entire region of incompressible deformation, whereas here in Fig. 11 the stability check is just performed along the three prototype deformations by evaluating (14) – (16) mentioned in the ABAQUS Manual [2].

In contrast and extension to that, here we give the results by exploring (13) and thus apply the evaluation of (8) for the whole region. As can be seen, all three methods end up in the exactly same results – here for the YEOH model.

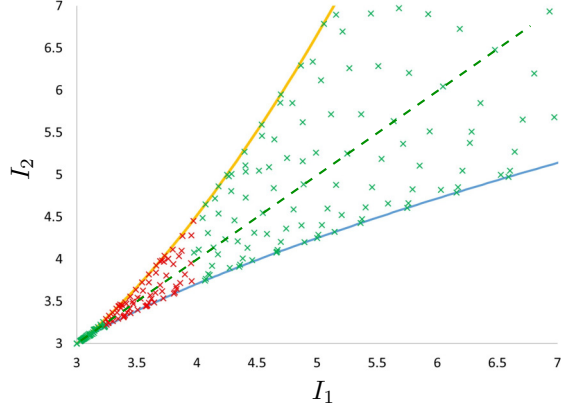


Figure 12: Plane of invariants as scope for visualization of the stability check using $\mathbb{D} \in \text{Sym}^{++}(2)$ of (8) in the entire region for the YEOH model with the parameters in Tab. 1.

4 Conclusions

We have succeeded in developing a uniform representation and a standardized procedure that makes it possible to visualize material stability for the incompressible isotropic hyperelasticity model class and its prototype deformation modes in an overall picture. A similar procedure (presumably numerically) is also used in commercial FE-codes such as ABAQUS or ANSYS to warn of potential instabilities during application. This is now also possible in a comprehensible and graphical way, and should definitely be included when adapting material properties to material samples or component measurements for industrial applications. It must be noted that deformation modes with rotating principal axes – the simple shear case is a good example – can fulfill the incompressible HILL stability condition $\mathbb{H}^{\text{inc}} \in \text{Sym}^{++}(2)$, but this does not guarantee monotonicity of the true shear stress–strain relationship in *simple shear*³, see [30], and therefore one should in addition require as useful stability condition the "LEGENDRE–HADAMARD–ellipticity" of the constitutive law, namely the condition $D_{\mathbf{F}}^2 W(\mathbf{F}) \cdot (\xi \otimes \eta, \xi \otimes \eta) > 0 \quad \forall \xi, \eta \neq 0$. This computation of HILL's stability requirement and the additional LH–ellipticity seems to be sufficient for excluding any sort of material instability in incompressible hyperelasticity and should therefore be routinely checked for FE–calculation in accordance with the findings in [30]. It remains to find a structure that a priori satisfies HILL's inequality **and** the LEGENDRE–HADAMARD ellipticity while being able to suitably fit experimental data. This will be pursued next in [21] using a neural network structure.

³We show in the Appendix E the relation between the shear component and the shear γ .

Conflict of interest

The author declares that he has no conflict of interest.

Acknowledgement

The author thanks PATRIZIO NEFF (Faculty of Mathematics, Univ. Duisburg–Essen, Germany) for in–depth discussions of pertinent stability concepts in incompressible isotropic hyperelasticity. Especially, the essential equivalence of \mathbb{H}^{inc} and \mathbb{D} as stability indicators in the Appendix D.3 is an outcome of this discussion, together with Appendixes C, D and E.

The author also thanks ATTILA KOSA (*Department of Applied Mechanics*, Budapest University of Technology and Economics) for sharing a detailed numerical discussion on the stability limits of the MOONEY–RIVLIN model.

A Derivations within the plane of invariants

A.1 A closed form representation of stretches versus invariants at incompressibility

In [18] the closed form representation of [43] is reformulated and given in order to obtain the stretches (λ_1, λ_2) from a given pair (\bar{I}_1, \bar{I}_2) for the incompressible case, i.e. $I_3 \equiv 1$. In a similar way, mathematically somewhat more complex, but also in closed form, one can obtain the representation [5] used here by (λ, m) from such a given pairing (λ_1, λ_2) or (\bar{I}_1, \bar{I}_2) , respectively. This will be demonstrated here as an example. Let us start with two substitutions in order to simplify our notation: We set

$$\mu := \lambda^2 \quad \text{and} \quad \eta := \mu^m \quad (40)$$

to obtain the given invariants (\bar{I}_1, \bar{I}_2) from (3) as

$$\bar{I}_1 = \mu + \eta + \frac{1}{\mu \eta} \quad \text{and} \quad \bar{I}_2 = \frac{1}{\mu} + \frac{1}{\eta} + \mu \eta. \quad (41)$$

Here, (41)₁ represents the quadratic equation $\mu \eta^2 + (\mu^2 - \bar{I}_1 \mu) \eta + 1 = 0$ for η , whose solution is given by

$$\eta_{1,2} = \frac{(\bar{I}_1 \mu - \mu^2) \pm \sqrt{\mu^4 - 2\bar{I}_1 \mu^3 + \bar{I}_1^2 \mu^2 - 4\mu}}{2\mu} = \mu^m. \quad (42)$$

On the other hand, (41)₂ provides the cubic representation $\mu^3 - \bar{I}_1 \mu^2 + \bar{I}_2 \mu - 1 = 0$ in μ , which can be transformed by

$$p := +\bar{I}_2 - \frac{\bar{I}_1^2}{3} \quad \text{and} \quad q := +\frac{\bar{I}_1 \bar{I}_2}{3} - \frac{2}{27} \bar{I}_1^3 - 1 \quad (43)$$

into the *reduced cubic equation* $z^3 + pz + q = 0$ with $z := \mu - \frac{\bar{I}_1}{3}$. In our case, this equation has three real solutions, where we bypass the complex solutions using $\rho := \sqrt{-p^3/27}$ and $\cos \varphi = -q/2\rho$. This gives us $z_1 = 2\sqrt[3]{\rho} \cos(\varphi/3)$ as the first of the three solutions, from which $\mu = \lambda^2$ follows directly.

With $\eta^+ = \mu^m$ from (42)₁ we have

$$\log \eta^+ = m \log \mu \quad (44)$$

and therefore $m = \frac{\log \eta^+}{\log \mu}$ from that derivations. This allows us to convert any representation into a correspondingly different one, even if it involves nonlinear equations up to the 3rd order.

A.2 Analytical derivation of boundary lines in the plane of invariants

We give the analytical derivation of the functions $\bar{I}_2 = \bar{I}_2(\bar{I}_1)$ representing the boundary lines of possible deformation modes in the plane of invariants, see Fig. 1. The two boundary lines for the uniaxial and the biaxial deformation mode, respectively, are obtained using (2).

From (2)₁ with $\lambda_1 = \lambda$ and $\lambda_2 = \lambda^{-\frac{1}{2}}$ we see

$$\lambda^3 - \bar{I}_1 \lambda + 2 = 0, \quad (45)$$

which can be solved for λ directly applying CARDANO's formula. Assigning $p := -\bar{I}_1$, $q := 2$ and therefore $D = 1 - \bar{I}_1^3/27 < 0$, we receive

$$\varphi = \frac{1}{3} \arccos \left[-\sqrt{27/\bar{I}_1^3} \right] \quad (46)$$

and from this the stretch

$$\lambda = 2 \sqrt{\frac{\bar{I}_1}{3}} \cos \varphi. \quad (47)$$

Using that result in (2)₂ we obtain

$$I_2 = 4 \sqrt{\frac{\bar{I}_1}{3}} \cos \varphi + \frac{3}{4 \bar{I}_1 \cos^2 \varphi}, \quad (48)$$

which represents (with φ from (46)) the uniaxial boundary line $\bar{I}_2(\bar{I}_1)$ and has already been published in [5]. The boundary line for the biaxial mode is obtained in the same way from (2) with $\lambda_1 = \lambda_2 = \lambda$.

In addition, we again give the *plane of invariants* with the boundary lines (48) from above and points of data pairs (\bar{I}_1, \bar{I}_2) in blue representing a set of possible deformations generated by a sequence of randomly produced deformation gradients \mathbf{F} with $J = \det \mathbf{F} \equiv 1$.

Furthermore, one might ask what happens if one chooses values of m in the family $\mathbf{F} = \text{diag}(\lambda, \lambda^m, \lambda^{-(m+1)})$ that lie outside of the interval $m \in (-\frac{1}{2}, 1)$.

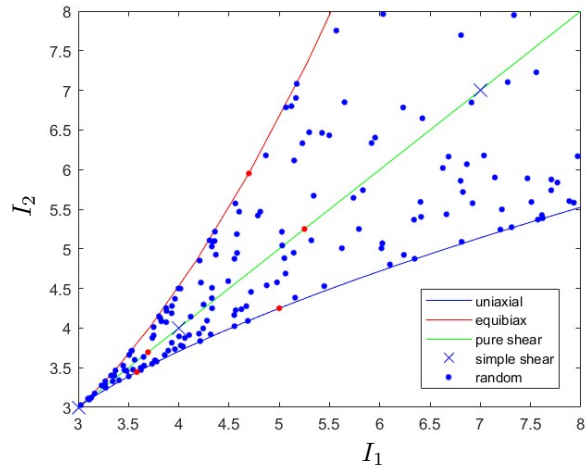


Figure 13: Plot and derivation of *plane of invariants* with randomly generated points of possible incompressible deformations in blue.

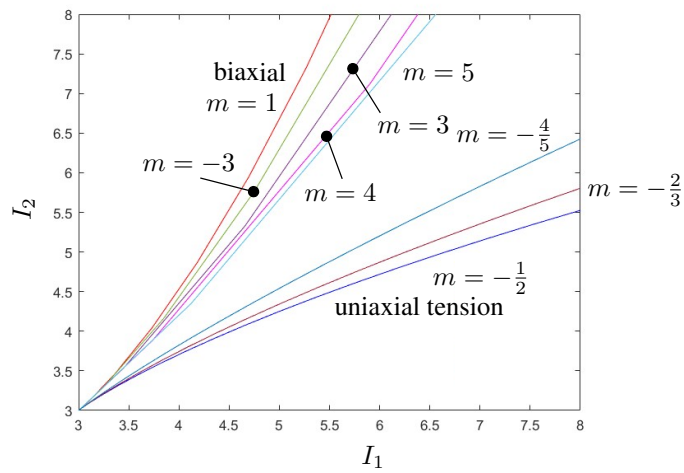


Figure 14: Plot of deformation paths for arbitrary m in the plane of invariants.

Here, we show the path of different m in the plane of invariants as an example, see Fig. 14.

If we now consider a possible deformation path within that family, we see that such situations can be interpreted as a sequence of successive prototype deformations

$$\mathbf{F}_{(m=4)} = \begin{bmatrix} \lambda & 0 & 0 \\ 0 & \lambda^4 & 0 \\ 0 & 0 & \lambda^{-5} \end{bmatrix} = \underbrace{\begin{bmatrix} \lambda & 0 & 0 \\ 0 & \lambda & 0 \\ 0 & 0 & \lambda^{-2} \end{bmatrix}}_{\text{biax}} \cdot \underbrace{\begin{bmatrix} 1 & 0 & 0 \\ 0 & \lambda^3 & 0 \\ 0 & 0 & \lambda^{-3} \end{bmatrix}}_{\text{multiple pure shear}} \quad (49)$$

by a multiplicative decomposition of \mathbf{F} , see [24] or [19].

Here, we again refer to Fig. 3, where we have shown the equivalence of m and m^* in tension and compression, i.e. $\lambda > 1$ and $\lambda < 1$, and vice versa. Reformulating (41) from above, we obtain a quadratic equation in μ with the solutions $\mu_{1,2}$ and the cubic equation

$$\eta^3 - I_1\eta^2 + I_2\eta - 1 = 0 \quad (50)$$

in $\eta = \mu^m$ with the at first three possible solutions $\eta_{1,2,3}$. In consequence, we have a set of six possible solution of (50), i.e. $\eta_{1,2,3} = \mu_{1,2}^{m_{1,2,3}}$. Unfortunately, we cannot yet provide a further analytical solution. Therefore, we are currently reliant on a numerical solution and a comparison of possible meaningful results.

This comparison yields only one meaningful m^* for $\lambda \in (0.1, 1)$ and a given, fixed mode parameter m , where we exclude $m^* = m$ and $m^* = 0$ as solutions. At this point, we define the here resulting m^* as equivalent to the given m as depicted in Fig. 3.

B MATLAB code for the stress computation

Here we give the MATLAB code to calculate the two stress components from (11) in order to reproduce the ABAQUS stability criterion according to (8):

```
clear all
syms lam1 lam2 lam3 I1 I2 c1 c2 c3

W_Yeoh = c1*(I1-3) + c2*(I1-3)^2 + c3*(I1-3)^3
dW_dI1 = diff(W_Yeoh,I1);
dW_dI2 = diff(W_Yeoh,I2);

%
I1 = lam1^2+lam2^2+lam3^2
dW_dI1 = subs(dW_dI1,I1,1);
I2 = lam1^2*lam2^2+lam1^2*lam3^2+lam2^2*lam3^2
dW_dI2 = subs(dW_dI2,I2,1);

%
% sig3 == 0
```

```

p = 2*lam3^2*dW_dI1 + 2*(lam1^2*lam3^2+lam2^2*lam3^2)*dW_dI2;

sig1 = lam1*2*lam1*dW_dI1 + lam1*(2*lam1*lam2^2+2*lam1*lam3^2)*dW_dI2 - p;
sig2 = lam2*2*lam2*dW_dI1 + lam2*(2*lam1^2*lam2+2*lam2*lam3^2)*dW_dI2 - p;

% Incompressibility: lam3 = 1/lam1/lam2
sig1 = subs(sig1, lam3, 1/lam1/lam2)
sig2 = subs(sig2, lam3, 1/lam1/lam2)

% ABAQ - multiplication by lam_i is equiv. to D_log(.)
DD_11 = simplify( expand( lam1*diff(sig1, lam1) ) );
DD_12 = simplify( expand( lam2*diff(sig1, lam2) ) );
DD_21 = simplify( expand( lam1*diff(sig2, lam1) ) );
DD_22 = simplify( expand( lam2*diff(sig2, lam2) ) );

det = DD_11*DD_22 - DD_12*DD_21
trc = DD_11+DD_22

% uniax
det_1ax = subs(det, lam2, lam1^(-1/2))
trc_1ax = subs(trc, lam2, lam1^(-1/2))

% PS
det_PS = subs(det, lam2, 1)
trc_PS = subs(trc, lam2, 1)

% biax
det_biax = subs(det, lam2, lam1)
trc_biax = subs(trc, lam2, lam1)

```

Getting these expressions in analytical form, we are able to plot the results depending on the parameters c_1, c_2, c_3 .

C Evaluation of HILL's condition in rate-form

In continuation of (18) in rate-form adapting a calculation from [30], Sect. 4.2, HILL's inequality for diagonal deformation states amounts to

$$0 < \left\langle \frac{D^{ZJ}\boldsymbol{\tau}}{Dt}, \mathbf{d} \right\rangle = \left\langle \frac{\partial \boldsymbol{\tau}}{\partial t}, \mathbf{d} \right\rangle = \sum_{i=1}^3 \partial_t [\tau_i(\lambda_1(t), \lambda_2(t), \lambda_3(t))] \frac{\dot{\lambda}_i(t)}{\lambda_i(t)}, \quad (51)$$

where we obtain the rate $\mathbf{d} = \text{sym } \mathbf{l} = \frac{1}{2}(\mathbf{l} + \mathbf{l}^T)$ from $\mathbf{l} = \dot{\mathbf{F}} \cdot \mathbf{F}^{-1}$ here with

$$\mathbf{F} = \text{diag}(\lambda(t), \lambda^m(t), \lambda^{-m-1}(t)) \quad (52)$$

and $\det \mathbf{F} = 1$ resulting in

$$\dot{\mathbf{F}} = \text{diag} \left(\dot{\lambda}(t), m \lambda^{m-1}(t) \dot{\lambda}(t), (-m-1) \lambda^{-m-2} \dot{\lambda}(t) \right) \quad (53)$$

and therefore

$$\begin{aligned} \mathbf{d} &= \text{diag} \left(\frac{\dot{\lambda}(t)}{\lambda(t)}, m \frac{\lambda^{m-1}}{\lambda^m} \dot{\lambda}(t), (-m-1) \frac{\lambda^{-m-2}}{\lambda^{-m-1}} \dot{\lambda}(t) \right) \\ &= \text{diag} \left(\frac{\dot{\lambda}(t)}{\lambda(t)}, m \frac{\dot{\lambda}(t)}{\lambda(t)}, (-m-1) \frac{\dot{\lambda}(t)}{\lambda(t)} \right) \\ &= \frac{\dot{\lambda}(t)}{\lambda(t)} \text{diag}(1, m, -(m+1)) \quad \text{with } \text{trace}(\mathbf{d}) = 0. \end{aligned} \quad (54)$$

Going on, (51) writes now as

$$\begin{aligned} 0 &< \left\langle \frac{\partial \boldsymbol{\tau}}{\partial t}, \mathbf{d} \right\rangle = \frac{\partial \boldsymbol{\tau}}{\partial t} : \mathbf{d} = \partial_t [\tau_1(\cdot)] \frac{\dot{\lambda}(t)}{\lambda(t)} + \partial_t [\tau_2(\cdot)] m \frac{\dot{\lambda}(t)}{\lambda(t)} - \partial_t [\tau_3(\cdot)] (m+1) \frac{\dot{\lambda}(t)}{\lambda(t)} \\ &= (\partial_t [\tau_1(\cdot)] + m \partial_t [\tau_2(\cdot)] - (m+1) \partial_t [\tau_3(\cdot)]) \frac{\dot{\lambda}}{\lambda} \\ &= (\partial_t [\tau_1(\lambda, \lambda^m, \lambda^{-m-1})] + \partial_t [\tau_2(\lambda, \lambda^m, \lambda^{-m-1})] + \partial_t [\tau_3(\lambda, \lambda^m, \lambda^{-m-1})]) \frac{\dot{\lambda}}{\lambda}. \end{aligned} \quad (55)$$

We define

$$\begin{aligned} \hat{\tau}_1(\lambda(t)) &:= \tau_1(\lambda(t), \lambda^m(t), \lambda^{-m-1}(t)), \\ \hat{\tau}_2(\lambda(t)) &:= \tau_2(\lambda(t), \lambda^m(t), \lambda^{-m-1}(t)), \\ \hat{\tau}_3(\lambda(t)) &:= \tau_3(\lambda(t), \lambda^m(t), \lambda^{-m-1}(t)) \end{aligned} \quad (56)$$

and observe that $\partial_t [\hat{\tau}_i(\lambda(t))] = D_\lambda \hat{\tau}_i(\lambda(t)) \dot{\lambda}(t)$ continuing further

$$\begin{aligned} 0 < \left\langle \frac{\partial \boldsymbol{\tau}}{\partial t}, \mathbf{d} \right\rangle &= \left\{ D_\lambda \hat{\tau}_1(\lambda) \dot{\lambda} + m D_\lambda \hat{\tau}_2(\lambda) \dot{\lambda} - (m+1) D_\lambda \hat{\tau}_3(\lambda) \dot{\lambda} \right\} \frac{\dot{\lambda}}{\lambda} \\ &= \{D_\lambda \hat{\tau}_1(\lambda) + m D_\lambda \hat{\tau}_2(\lambda) - (m+1) D_\lambda \hat{\tau}_3(\lambda)\} \underbrace{\frac{\dot{\lambda}}{\lambda}}_{>0}. \end{aligned} \quad (57)$$

Let us check the three prototype modes of deformation

uniaxial tension	with $m = -\frac{1}{2}$,	$\mathbf{F} = \text{diag}(\lambda, \lambda^{-\frac{1}{2}}, \lambda^{-\frac{1}{2}})$	and $\tau_2 = \tau_3 = 0$
pure shear	with $m = 0$,	$\mathbf{F} = \text{diag}(\lambda, 1, \lambda^{-1})$	and $\tau_3 = 0$
\Leftrightarrow plane strain	with $\lambda_2 = 1$ fixed		
\Leftrightarrow planar tension			
biaxial tension	with $m = 1$,	$\mathbf{F} = \text{diag}(\lambda, \lambda, \lambda^{-2})$	and $\tau_1 = \tau_2, \tau_3 = 0$.

In all three cases, fully considering the stress–boundary conditions, we obtain

$$0 < \left\langle \frac{\partial \boldsymbol{\tau}}{\partial t}, \mathbf{d} \right\rangle \iff \underbrace{D_\lambda \hat{\tau}_1(\lambda)}_{\text{positive incremental moduli}} > 0 \quad (58)$$

and HILL’s inequality is satisfied if and only if $D_\lambda \hat{\tau}_1(\lambda) > 0$. This means along these special deformation states, HILL’s inequality amounts to a positive incremental modulus $D_\lambda \hat{\tau}_1(\lambda)$. Indeed, this stability concept is already used in [23] for the MOONEY–RIVLIN model.

Along the family $\mathbf{F} = \text{diag}(\lambda, \lambda^m, \lambda^{-(m+1)})$ we can always assume that the stretch in the third component adjusts itself freely due to incompressibility once the first two components are set. Thus, HILL’s inequality along the family $\mathbf{F} = \text{diag}(\lambda, \lambda^m, \lambda^{-(m+1)})$ reads, continuing from (57),

$$0 < \left\langle \frac{\partial \boldsymbol{\tau}}{\partial t}, \mathbf{d} \right\rangle = \underbrace{(D_\lambda \hat{\tau}_1(\lambda) + m D_\lambda \hat{\tau}_2(\lambda) - (m+1) D_\lambda \hat{\tau}_3(\lambda))}_{=: D_{1D}^m} \frac{|\dot{\lambda}|^2}{\lambda}. \quad (59)$$

This motivates to consider the generalized incremental modulus

$$D_{1D}^m := D_\lambda \hat{\tau}_1(\lambda) + m D_\lambda \hat{\tau}_2(\lambda) - (m+1) D_\lambda \hat{\tau}_3(\lambda), \quad (60)$$

and HILL’s inequality along the family $\mathbf{F} = \text{diag}(\lambda, \lambda^m, \lambda^{-(m+1)})$ is satisfied, if and only if $D_{1D}^m > 0$. The stress boundary condition for $\hat{\tau}_2$ and $\hat{\tau}_3$ has to be incorporated, see the three prototype examples following (13). In our algorithmic treatment we check the latter condition for $m \in [-\frac{1}{2}; 1]$, thus extending the necessary ABAQUS check from the prototype modes to the family $\mathbf{F} = \text{diag}(\lambda, \lambda^m, \lambda^{-(m+1)})$. However, the condition

$$D_{1D}^m > 0 \quad \forall m \in [-\frac{1}{2}, 1] \quad (61)$$

does not imply HILL’s inequality for the incompressible case in general⁴. This is shown exemplary in Fig. 8 in contrast to Fig. 17, where firstly (61) is applied above and, secondly, HILL’s inequality in the form of (74) is used. Nevertheless, the aim of this article is to show the application of the 1D condition (61) for simplified and quick stability estimations in the case of incompressible deformation modes.

D Another view on the MOONEY–RIVLIN model (33): comparison of stability checks

This section describes a generalized version of the MOONEY–RIVLIN model (33) in order to add statements about the convexity of this type of energy functions

⁴This situation is similar to a scalar function, which is convex along a family of straight slices which cover its domain of definition, but the function is not convex over its domain of definition.

with I_1 and I_2 . To this end, let us consider the function

$$W_{\text{MoRi}} = c_1 (I_1 - 3) + c_2 (I_2 - 3) = c_1 (\|\mathbf{v}\|^2 - 3) + c_2 (\|\mathbf{v}^{-1}\|^2 - 3) \quad (62)$$

with the left stretch tensor $\mathbf{v} = \mathbf{F} \cdot \mathbf{R}^{-1}$, the material parameters c_1 , c_2 and the condition $\det \mathbf{v} = 1$ for incompressibility. With reference to HILL[16] (page 469) and reformulating the parameters μ and δ given there, one can write (62) in the form

$$W_{\text{MoRi}} = \frac{1}{2}\mu\left(\frac{1}{2} + \delta\right)(\|\mathbf{v}\|^2 - 3) + \frac{1}{2}\mu\left(\frac{1}{2} - \delta\right)(\|\mathbf{v}^{-1}\|^2 - 3) \quad (63)$$

by $\mu = 2(c_1 + c_2)$ and $\delta = \frac{c_1 - c_2}{2(c_1 + c_2)} = \frac{c_1 - c_2}{\mu}$ with the parameters as given in (62). HILL himself ([16], p. 496) gives the limit $|\delta| \leq \frac{1}{2}$ for an overall HILL'S inequality to be satisfied. This means, the prefactors of the two energy terms, i.e. the material parameters, must be positive for HILL'S inequality to be satisfied. From (62), we obtain furtheron

$$\begin{aligned} W_{\text{MoRi}} &= c_1 (\|e^{\log \mathbf{v}}\|^2 - 3) + c_2 (\|e^{-\log \mathbf{v}}\|^2 - 3) \\ &= c_1 ([e^{2x_1} + e^{2x_2} + e^{2x_3}] - 3) + c_2 ([e^{-2x_1} + e^{-2x_2} + e^{-2x_3}] - 3) \\ &=: \widehat{W}(x_1, x_2, x_3), \end{aligned} \quad (64)$$

where $x_i := \log \lambda_i$, ($i = 1, 2, 3$) are the "principal log-stretches". From that we directly compute the principal KIRCHHOFF stresses

$$\tau_i = \frac{d\widehat{W}}{dx_i} = \frac{d\widehat{W}}{d\log \lambda_i} \quad (65)$$

in equivalence to (25), which is used in the following development.

D.1 Checking HILL'S inequality in the general compressible case

Checking the convexity of \widehat{W} as a function of $\log \mathbf{v}$ is easy by considering the HESSE matrix $\mathbb{H} := D^2\widehat{W} \in \text{Sym}(3)$. Based on (65) this step gives us the HESSE matrix in general form

$$\begin{aligned} \mathbb{H} &= \begin{bmatrix} H_{11} & H_{12} & H_{13} \\ H_{12} & H_{22} & H_{23} \\ H_{13} & H_{23} & H_{33} \end{bmatrix} = \left(\frac{\partial^2 \widehat{W}(x_1, x_2, x_3)}{\partial x_i \partial x_j} \right)_{i,j=1,2,3} \quad (66) \\ &= \begin{bmatrix} \frac{\partial^2 \widehat{W}}{\partial x_1 \partial x_1} & \frac{\partial^2 \widehat{W}}{\partial x_1 \partial x_2} & \frac{\partial^2 \widehat{W}}{\partial x_1 \partial x_3} \\ \frac{\partial^2 \widehat{W}}{\partial x_2 \partial x_1} & \frac{\partial^2 \widehat{W}}{\partial x_2 \partial x_2} & \frac{\partial^2 \widehat{W}}{\partial x_2 \partial x_3} \\ \frac{\partial^2 \widehat{W}}{\partial x_3 \partial x_1} & \frac{\partial^2 \widehat{W}}{\partial x_3 \partial x_2} & \frac{\partial^2 \widehat{W}}{\partial x_3 \partial x_3} \end{bmatrix} = \begin{bmatrix} \frac{\partial \tau_1}{\partial x_1} & \frac{\partial \tau_1}{\partial x_2} & \frac{\partial \tau_1}{\partial x_3} \\ \frac{\partial \tau_2}{\partial x_1} & \frac{\partial \tau_2}{\partial x_2} & \frac{\partial \tau_2}{\partial x_3} \\ \frac{\partial \tau_3}{\partial x_1} & \frac{\partial \tau_3}{\partial x_2} & \frac{\partial \tau_3}{\partial x_3} \end{bmatrix} \quad \text{with } \boldsymbol{\tau} = D_{\log \mathbf{v}} \widehat{W}(\log \mathbf{v}). \end{aligned}$$

It is clear that if \mathbb{H} is positive definite, the energy function W is convex as a function of $\log \lambda_i$ and this convexity remains true also along the subset $\det \mathbf{F} = 1$ of incompressible deformations since $1 = \det \mathbf{F} \iff \text{trace}(\log \mathbf{v}) = 0$ is a linear and convex subset in the log-space. We may evaluate the positive definiteness of \mathbb{H} with SYLVESTER'S criterion

$$H_{11} > 0, \quad H_{11} \cdot H_{22} - H_{12} \cdot H_{21} \quad \text{and} \quad \det \mathbb{H} > 0 \quad (67)$$

or

$$\text{trace}(\mathbb{H}) > 0, \quad \text{trace}(\text{Cof } \mathbb{H}) > 0, \quad \det \mathbb{H} > 0 \quad (68)$$

along the incompressible family $\mathbf{F} = \text{diag}(\lambda, \lambda^m, \lambda^{-(m+1)})$ leading with the parameter set $c_1 = 0.8 \text{ MPa}$ and $c_2 = -0.2 \text{ MPa}$ to Fig. 15, while the evaluation for D_{1D}^m (from (60)) gives a different result shown in Fig. 8.

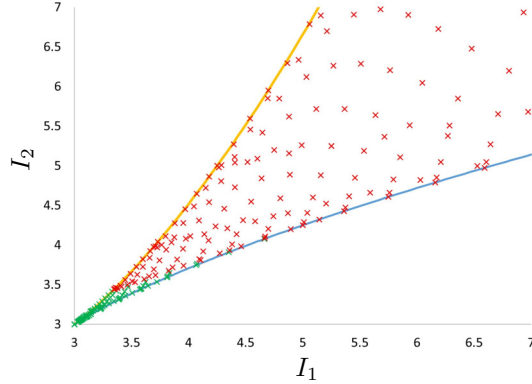


Figure 15: Plane of invariants as scope for visualization the material stability of the MOONEY–RIVLIN model (64) with the parameter set $c_1 = 0.8 \text{ MPa}$ and $c_2 = -0.2 \text{ MPa}$: The green crosses here mark the stable region as defined by the condition based on positive definiteness of \mathbb{H} in (67) without taking special care of the incompressibility assumption.

D.2 Checking HILL'S inequality in the general incompressible case: the projected HESSE matrix \mathbb{H}^{inc}

In the log-space, the incompressibility constraint translates to $\log \lambda_1 + \log \lambda_2 + \log \lambda_3 = 0 \Leftrightarrow \lambda_1 \lambda_2 \lambda_3 = 1$. Abbreviating $x_i = \log \lambda_i$, we need to evaluate

$$\left\langle D^2 \widehat{W}(x_1, x_2, x_3) \cdot \eta, \eta \right\rangle > 0 \quad \forall \eta \neq 0, \quad \eta_1 + \eta_2 + \eta_3 = 0. \quad (69)$$

The linear subspace

$$\eta_1 + \eta_2 + \eta_3 = 0 \quad (70)$$

is a plane with normal vector $\mathbf{n} = \begin{bmatrix} 1 \\ 1 \\ 1 \end{bmatrix}$ as depicted in Fig. 16. This plane is spanned by (70) as $\mathbf{u} = \begin{bmatrix} 0 \\ -1 \\ 1 \end{bmatrix}$ and $\mathbf{v} = \begin{bmatrix} 1 \\ -1 \\ 0 \end{bmatrix}$. Thus we can write any vector $\boldsymbol{\eta}$ satisfying (70) as

$$\boldsymbol{\eta} = \xi_1 \mathbf{u} + \xi_2 \mathbf{v} = \begin{bmatrix} 0 & 1 \\ -1 & -1 \\ 1 & 0 \end{bmatrix} \cdot \begin{bmatrix} \xi_1 \\ \xi_2 \end{bmatrix} = \mathbf{P} \cdot \begin{bmatrix} \xi_1 \\ \xi_2 \end{bmatrix}. \quad (71)$$

Therefore, (69) rewrites as

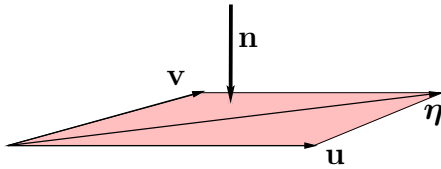


Figure 16: Every vector $\boldsymbol{\eta}$ in the plane (70) can be represented as $\boldsymbol{\eta} = \mathbf{P} \cdot \boldsymbol{\xi}$.

$$\begin{aligned} \left\langle \mathbf{D}^2 \widehat{W}(x_1, x_2, x_3) \cdot \boldsymbol{\eta}, \boldsymbol{\eta} \right\rangle_{\mathbb{R}^3} &= \left\langle \mathbf{D}^2 \widehat{W}(x_1, x_2, x_3) \cdot \mathbf{P} \cdot \begin{bmatrix} \xi_1 \\ \xi_2 \end{bmatrix}, \mathbf{P} \cdot \begin{bmatrix} \xi_1 \\ \xi_2 \end{bmatrix} \right\rangle_{\mathbb{R}^3} \\ &= \left\langle \mathbf{P}^T \cdot \mathbf{D}^2 \widehat{W}(x_1, x_2, x_3) \cdot \mathbf{P} \cdot \begin{bmatrix} \xi_1 \\ \xi_2 \end{bmatrix}, \begin{bmatrix} \xi_1 \\ \xi_2 \end{bmatrix} \right\rangle_{\mathbb{R}^2} > 0 \quad \forall (\xi_1, \xi_2) \in \mathbb{R}^2 \neq 0. \end{aligned} \quad (72)$$

Accordingly, we check the positive definiteness of the *projected HESSE matrix*

$$\mathbb{H}^{\text{inc}} := \mathbf{P}^T \cdot \mathbb{H} \cdot \mathbf{P} = \begin{bmatrix} H_{11} - 2H_{12} + H_{22} & H_{13} - H_{12} + H_{22} - H_{23} \\ H_{13} - H_{12} + H_{22} - H_{23} & H_{22} - 2H_{23} + H_{33} \end{bmatrix} \quad (73)$$

in the following. It is now clear, that

$$\begin{aligned} \mathbb{H}^{\text{inc}} \in \text{Sym}^{++}(2) &\iff \{\mathbb{H}^{\text{inc}}\}_{11} > 0 \quad \text{and} \quad \det \mathbb{H}^{\text{inc}} > 0 \\ &\iff \text{trace}(\mathbb{H}^{\text{inc}}) > 0 \quad \text{and} \quad \det \mathbb{H}^{\text{inc}} > 0 \end{aligned} \quad (74)$$

is the final encompassing condition of HILL's inequality in the incompressible case, see Fig. 17. Subsequently we will show that this condition coincides with the ABAQUS check $\mathbb{D} \in \text{Sym}^{++}(2)$ of (8). Note again that $\mathbb{H}^{\text{inc}} \in \text{Sym}^{++}(2)$ is sufficient for $D_{1D}^m > 0$, but not the other way round, implying that the stability limits calculated based on $D_{1D}^m > 0$ are larger than those calculated for $\mathbb{H}^{\text{inc}} \in \text{Sym}^{++}(2)$, see (77) and Table 5⁵.

⁵As will be seen, HILL's incompressible inequality condition $\mathbb{H}^{\text{inc}} \in \text{Sym}^{++}(2)$ (*) is equivalent to the ABAQUS DRUCKER condition. This can be evaluated for the MOONEY–RIVLIN model

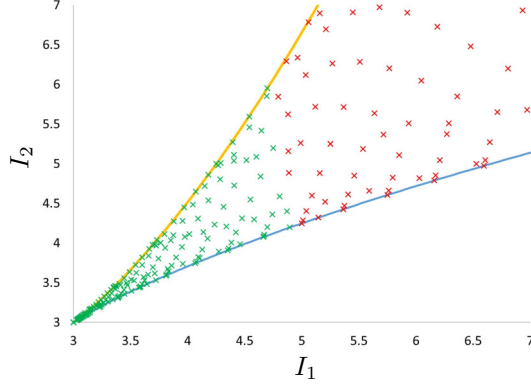


Figure 17: Plane of invariants as scope for visualization the material stability of the MOONEY–RIVLIN model (64) with the parameter set $c_1 = 0.8$ MPa and $c_2 = -0.2$ MPa. The green crosses here mark the complete stable region as defined by the condition based on positive definiteness of \mathbb{H}^{inc} in (67), which show a larger green (i.e. stable) area compared to Fig. 15 above.

in certain deformation states, e.g. a deformation shown in uniaxial tension. There, no use is made of stress boundary conditions, i.e. it is irrelevant, how we got uniaxial tension geometry. On the other hand, another condition is e.g. looking at uniaxial tension, incorporating the stress condition, and then requiring monotonicity of CAUCHY stress versus stretch: $D_{1D}^m > 0$ (**). Now it holds $(*) \Rightarrow (**)$, but not the other way round. Therefore, the limits calculated from (**) are larger than the limits calculated from (*), while both have been calculated for the geometry of uniaxial tension, see Table 5.

In contrast, the built-in ABAQUS stability check gives a stable situation for the three prototype deformations and the MOONEY–RIVLIN model using the discussed parameter set $c_1 = 0.8$ MPa and $c_2 = -0.2$ MPa in the range of

$$\begin{aligned}\varepsilon_{\text{uniax}} &\in (-0.5614...1.00) \iff \lambda \in (0.4386...2), \\ \varepsilon_{\text{pure shear}} &\in (-0.4737...0.99) \iff \lambda \in (0.5263...1.9), \\ \varepsilon_{\text{biax}} &\in (-0.2919...0.51) \iff \lambda \in (0.7071...1.51)\end{aligned}$$

for the nominal strains $\varepsilon = \lambda - 1$. The output of ABAQUS material (stability) evaluation is given by

HYPERELASTICITY – MOONEY–RIVLIN STRAIN ENERGY

$$\begin{array}{cc} C1 & C2 \\ 0.8 & -0.2 \end{array}$$

***WARNING: UNSTABLE HYPERELASTIC MATERIAL

UNIAXIAL TENSION:	UNSTABLE AT A NOMINAL STRAIN LARGER THAN	1.0000
UNIAXIAL COMPRESSION:	UNSTABLE AT A NOMINAL STRAIN LESS THAN	-0.5614
BIAXIAL TENSION:	UNSTABLE AT A NOMINAL STRAIN LARGER THAN	0.5100
BIAXIAL COMPRESSION:	UNSTABLE AT A NOMINAL STRAIN LESS THAN	-0.2929
PLANAR TENSION:	UNSTABLE AT A NOMINAL STRAIN LARGER THAN	0.9000
PLANAR COMPRESSION:	UNSTABLE AT A NOMINAL STRAIN LESS THAN	-0.4737

whereas the here given boundary values $\varepsilon_{\text{uniax}} = -0.5614$, $\varepsilon_{\text{pure shear}} = \varepsilon_{\text{planar compression}} = -0.4737$ and $\varepsilon_{\text{biax}} = -0.2929$ can be exactly reproduced by (8) for the MOONEY–RIVLIN model (33) applying the coefficients of \mathbb{D} to obtain $\lambda = \varepsilon_* + 1$ for that model in the form

$$\begin{aligned}D_{11} &= 4(\lambda_1^2 + \lambda_3^2)(c_1 + \lambda_2^2 c_2), \\ D_{22} &= 4(\lambda_2^2 + \lambda_3^2)(c_1 + \lambda_1^2 c_2), \\ D_{12} = D_{21} &= 4\lambda_3^2 c_1 + 4\lambda_3^{-2} c_2\end{aligned}\tag{75}$$

directly as given in [1] for the incompressible case for any strain energy density functions $W = W(\bar{I}_1, \bar{I}_2)$

$$\begin{aligned}D_{11} &= 4(\lambda_1^2 + \lambda_3^2)\left(\frac{\partial W}{\partial \bar{I}_1} + \lambda_2^2 \frac{\partial W}{\partial \bar{I}_2}\right) + 4(\lambda_1^2 - \lambda_3^2)^2\left(\frac{\partial^2 W}{\partial \bar{I}_1^2} + 2\lambda_2^2 \frac{\partial^2 W}{\partial \bar{I}_1 \partial \bar{I}_2} + \lambda_2^4 \frac{\partial^2 W}{\partial \bar{I}_2^2}\right), \\ D_{22} &= 4(\lambda_2^2 + \lambda_3^2)\left(\frac{\partial W}{\partial \bar{I}_1} + \lambda_1^2 \frac{\partial W}{\partial \bar{I}_2}\right) + 4(\lambda_2^2 - \lambda_3^2)^2\left(\frac{\partial^2 W}{\partial \bar{I}_1^2} + 2\lambda_1^2 \frac{\partial^2 W}{\partial \bar{I}_1 \partial \bar{I}_2} + \lambda_1^4 \frac{\partial^2 W}{\partial \bar{I}_2^2}\right), \\ D_{12} = D_{21} &= 4\lambda_3^2 \frac{\partial W}{\partial \bar{I}_1} + 4\lambda_3^{-2} \frac{\partial W}{\partial \bar{I}_2} + 4(\lambda_1^2 - \lambda_3^2)(\lambda_2^2 - \lambda_3^2)\left(\frac{\partial^2 W}{\partial \bar{I}_1^2} + (\lambda_1^2 + \lambda_2^2) \frac{\partial^2 W}{\partial \bar{I}_1 \partial \bar{I}_2} + \lambda_1^2 \lambda_2^2 \frac{\partial^2 W}{\partial \bar{I}_2^2}\right).\end{aligned}\tag{76}$$

Checking $\mathbb{D} \in \text{Sym}^{++}(2)$ based on (76) results in Fig. 18. Summarizing, we give an overview in the following Tab. 5. With respect to Tab. 5, and ignoring

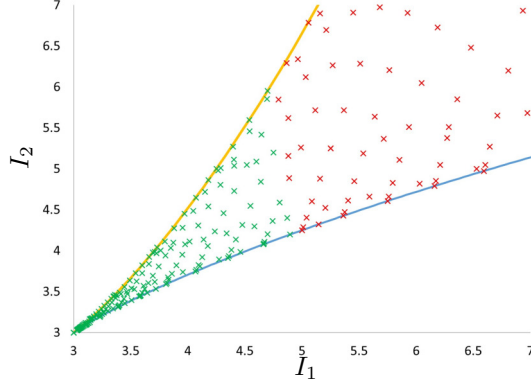


Figure 18: Plane of invariants as scope for visualization the material stability of the MOONEY–RIVLIN model (64) with the parameter set $c_1 = 0.8$ MPa and $c_2 = -0.2$ MPa. The green crosses here mark the complete stable region as defined by the condition based on positive definiteness of \mathbb{D} in (8) showing exactly the same result as Fig. 17 above, based on \mathbb{H}^{inc} .

	uniax mode	pure shear	biax
(67): $\mathbb{H} \in \text{Sym}^{++}(3)$	$\lambda \in (0.708\dots1.999)$	$\lambda \in (0.7072\dots1.4142)$	$\lambda \in (0.708\dots1.189)$
(73): $\mathbb{H}^{\text{inc}} \in \text{Sym}^{++}(2)$	$\lambda \in (0.4445\dots1.999)$	$\lambda \in (0.528\dots1.893)$	$\lambda \in (0.708\dots1.5)$
(8): $\mathbb{D} \in \text{Sym}^{++}(2)$	$\lambda \in (0.445\dots1.999)$	$\lambda \in (0.53\dots1.894)$	$\lambda \in (0.7072\dots1.5005)$
(60): $D_{1D}^m > 0$	$\lambda \in (0.4442\dots\infty)$	$\lambda \in (0\dots\infty)$	$\lambda \in (0\dots1.5)$
ABAQUS built-in	$\lambda \in (0.4386\dots2)$	$\lambda \in (0.5263\dots1.9)$	$\lambda \in (0.7071\dots1.51)$

Table 5: Comparison of the different stability ranges of the MOONEY–RIVLIN model with $c_1 = 0.8$ MPa and $c_2 = -0.2$ MPa for the various criteria from above wrt. the stretch $\lambda = \varepsilon + 1$ and the three prototype modes $m = -\frac{1}{2}, 0, 1$. Please note that regarding the accuracies of the third and fourth decimal places, it is evident that ABAQUS also uses a significantly higher accuracy than $\Delta\lambda = 0.01$ for this evaluation than is specified in the manual and previously cited in Sec. 2. While the lower and the upper stability limits based on \mathbb{H}^{inc} , \mathbb{D} and ABAQUS must be identical, different numerical implementations lead – in the view of the author – to slightly different values.

numerical errors, we observe for the three prototype modes $m = -\frac{1}{2}, 0, 1$ the

relations

$$\begin{aligned}
 \mathbb{H} &\in \text{Sym}^{++}(3) \\
 &\Downarrow \\
 \mathbb{H}^{\text{inc}} &\in \text{Sym}^{++}(2) \implies \mathbb{D} \in \text{Sym}^{++}(2) \\
 &\Downarrow \\
 \text{ABAQUS built-in check} &\implies D_{1D}^m > 0.
 \end{aligned} \tag{77}$$

To show a counter example for the MOONEY–RIVLIN model, we give an evaluation of the three stability criteria for that model with the parameter set $c_1 = 0.4$ MPa and $c_2 = -0.4$ MPa in Fig. 19, where for the three criteria each gives a different picture.

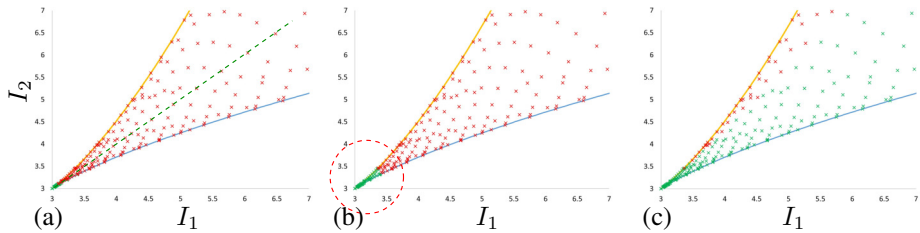


Figure 19: Summary for the MOONEY–RIVLIN model with the parameter set $c_1 = 1$ MPa and $c_2 = -0.4$ MPa based on (a) \mathbb{H} in (67), based on (b) \mathbb{H}^{inc} in (73) and on (c) D_{1D}^m in (32).

In addition to the discussion on the MOONEY–RIVLIN model above, here we summarize the representations of the YEOH model from Section 3.1 and supplement them with the derivations here concerning \mathbb{H} of (67) and \mathbb{H}^{inc} of (73).

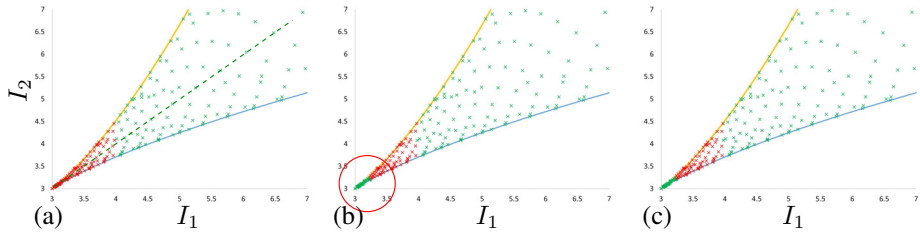


Figure 20: Summary for the Yeoh model with the parameter set $c_1 = 1$ MPa, $c_2 = -0.9$ MPa and $c_3 = 0.3$ MPa based on (a) \mathbb{H} in (67), based on (b) \mathbb{H}^{inc} in (73) and on (c) D_{1D}^m in (32), where (b) is equivalent to Fig. 12 and (c) is equivalent to Fig. 6.

D.3 Equivalence of positive definiteness for \mathbb{H}^{inc} and \mathbb{D}

As seen in the previous section, for the three prototype modes, the positive definiteness of \mathbb{H}^{inc} and of \mathbb{D} give the same stability limits. However, for a general strain state, the relation between \mathbb{H}^{inc} and \mathbb{D} is not clear at all at first sight.

On the one hand, we have from (73)

$$\begin{aligned} \mathbb{H}^{\text{inc}} &:= \mathbf{P}^T \cdot \mathbb{H} \cdot \mathbf{P} = \mathbf{P}^T \cdot D_{\log \lambda_i}^2 \widehat{W} \cdot \mathbf{P} \\ &= \begin{bmatrix} H_{22} - 2H_{23} + H_{33} & H_{13} - H_{12} + H_{22} - H_{23} \\ H_{13} - H_{12} + H_{22} - H_{23} & H_{11} - 2H_{12} + H_{22} \end{bmatrix} \quad \text{with} \quad \mathbf{P} = \begin{bmatrix} 0 & 1 \\ -1 & -1 \\ 1 & 0 \end{bmatrix}. \end{aligned} \quad (78)$$

On the other hand, it holds by assuming $\tau_2 = 0$ that (surprisingly, formula from PATRIZIO NEFF, *private communication*)

$$\begin{aligned} \widehat{\tau}_1 &= \partial_{\log \lambda_1} [W_{\text{red}}^{\text{inc}}(\lambda_1, \lambda_3)], \\ \widehat{\tau}_3 &= \partial_{\log \lambda_3} [W_{\text{red}}^{\text{inc}}(\lambda_1, \lambda_3)] \end{aligned} \quad (79)$$

so that

$$\begin{aligned} \overline{\mathbb{D}} &= \begin{bmatrix} D_{\log \lambda_1} \widehat{\tau}_1(\log \lambda_1, \log \lambda_3) & D_{\log \lambda_3} \widehat{\tau}_1(\log \lambda_1, \log \lambda_3) \\ D_{\log \lambda_1} \widehat{\tau}_3(\log \lambda_1, \log \lambda_3) & D_{\log \lambda_3} \widehat{\tau}_3(\log \lambda_1, \log \lambda_3) \end{bmatrix} \\ &= D_{\log \lambda_i}^2 [W_{\text{red}}^{\text{inc}}(\lambda_1, \lambda_3)] = D_{\log \lambda_i}^2 [\widehat{W}_{\text{red}}^{\text{inc}}(\log \lambda_1, \log \lambda_3)], \end{aligned} \quad (80)$$

where we have to set

$$\begin{aligned} W_{\text{red}}^{\text{inc}}(\lambda_1, \lambda_3) &:= W(\lambda_1, \frac{1}{\lambda_1 \lambda_3}, \lambda_3), \\ \widehat{W}_{\text{red}}^{\text{inc}}(\log \lambda_1, \log \lambda_3) &:= W_{\text{red}}^{\text{inc}}(e^{\log \lambda_1}, e^{\log \lambda_3}) \\ &= W(e^{\log \lambda_1}, e^{-(\log \lambda_1 + \log \lambda_3)}, e^{\log \lambda_3}) \end{aligned} \quad (81)$$

because of $\lambda_1^{-1} \lambda_3^{-1} = e^{-\log \lambda_1} e^{-\log \lambda_3} = e^{-(\log \lambda_1 + \log \lambda_3)}$. Let us write

$$\widehat{W}_{\text{red}}^{\text{inc}}(x_1, x_3) := W(e^{x_1}, e^{-(x_1 + x_3)}, e^{x_3}) = \widehat{W}(x_1, -(x_1 + x_3), x_3), \quad (82)$$

which gives for the HESSE matrix of $\widehat{W}_{\text{red}}^{\text{inc}}$

$$D_{(x_1, x_3)}^2 \widehat{W}_{\text{red}}^{\text{inc}}(x_1, x_3) = \begin{bmatrix} \delta_1 \delta_1 \widehat{W} - 2\delta_1 \delta_2 \widehat{W} + \delta_2 \delta_2 \widehat{W} & \delta_1 \delta_3 \widehat{W} - \delta_1 \delta_2 \widehat{W} - \delta_2 \delta_3 \widehat{W} + \delta_2 \delta_2 \widehat{W} \\ \delta_1 \delta_3 \widehat{W} - \delta_1 \delta_2 \widehat{W} - \delta_2 \delta_3 \widehat{W} + \delta_2 \delta_2 \widehat{W} & \delta_2 \delta_2 \widehat{W} - 2\delta_2 \delta_3 \widehat{W} + \delta_3 \delta_3 \widehat{W} \end{bmatrix}, \quad (83)$$

so that

$$\overline{\mathbb{D}} = \begin{bmatrix} H_{11} - 2H_{12} + H_{22} & H_{13} - H_{12} - H_{23} + H_{22} \\ H_{13} - H_{12} - H_{23} + H_{22} & H_{22} - 2H_{23} + H_{33} \end{bmatrix}. \quad (84)$$

Now, for isotropic response, the elastic energy W is invariant under permutations of the principal stretches. Therefore, the positive definiteness of \mathbb{D} from

(8) and the positive definiteness of $\bar{\mathbb{D}}$ from (84) are equivalent. Indeed, on the level of \mathbb{D} in (8) it is an arbitrary choice to require $\tau_3 = 0$. Here, we use instead $\tau_2 = 0$ for consistency. Comparing (84) and (79) we have shown that

$$\mathbb{H}^{\text{inc}} \in \text{Sym}^{++}(2) \iff \bar{\mathbb{D}} \in \text{Sym}^{++}(2) \quad (85)$$

since $\text{trace}(\mathbb{H}^{\text{inc}}) = \text{trace}(\bar{\mathbb{D}})$ and $\det \mathbb{H}^{\text{inc}} = \det \bar{\mathbb{D}}$. Thus

$$\mathbb{H}^{\text{inc}} \in \text{Sym}^{++}(2) \iff \mathbb{D} \in \text{Sym}^{++}(2) \quad (86)$$

and the ABAQUS stability check is shown to be fully equivalent to HILL's condition for the incompressible case.

E Non-monotonicity of the log shear measure in simple shear

Already for *simple shear* it can be shown that the shear components of the logarithmic strain tensor themselves exhibit a non-monotonic behavior with respect to the deformation $\gamma = \tan \alpha$, see Fig. 21 below. Here we give a closed form and derivation of $(\log \mathbf{b})_{12}$ in *simple shear* as function of γ .

Starting with the unique *polar decomposition* of the deformation gradient

$$\mathbf{F} = \mathbf{v} \cdot \mathbf{R} = \begin{bmatrix} 1 & \gamma & 0 \\ 0 & 1 & 0 \\ 0 & 0 & 1 \end{bmatrix} \quad (87)$$

in the *simple shear* case by an eigenvalue decomposition of

$$\mathbf{b} = \mathbf{F} \cdot \mathbf{F}^T = \begin{bmatrix} 1 + \gamma^2 & \gamma & 0 \\ \gamma & 1 & 0 \\ 0 & 0 & 1 \end{bmatrix} \quad (88)$$

by $(\mathbf{b} - \mu \mathbf{I}) \cdot \mathbf{n} = \mathbf{0}$ gives the eigenvalues of \mathbf{b} as

$$\mu_{1,2} = \left(\frac{\gamma \pm \sqrt{\gamma^2 + 4}}{2} \right)^2, \quad \mu_3 = 1, \quad (89)$$

see [20], and the three principal spatial directions

$$\mathbf{n}_1 = \begin{bmatrix} 2 \\ \sqrt{2\gamma^2 - 2\gamma\sqrt{\gamma^2 + 4} + 8} \\ -\gamma + \sqrt{\gamma^2 + 4} \\ \sqrt{2\gamma^2 - 2\gamma\sqrt{\gamma^2 + 4} + 8} \\ 0 \end{bmatrix}, \quad \mathbf{n}_2 = \begin{bmatrix} 2 \\ \sqrt{2\gamma^2 + 2\gamma\sqrt{\gamma^2 + 4} + 8} \\ -\gamma - \sqrt{\gamma^2 + 4} \\ \sqrt{2\gamma^2 + 2\gamma\sqrt{\gamma^2 + 4} + 8} \\ 0 \end{bmatrix} \quad \text{and} \quad \mathbf{n}_3 = \begin{bmatrix} 0 \\ 0 \\ 1 \end{bmatrix}, \quad (90)$$

which are mutually orthogonal and normalized, see [17] and [20]. From the author's point of view, this compact representation (90) is also rarely found in literature, while the decomposition for $\mathbf{C} = \mathbf{F}^T \cdot \mathbf{F}$ in contrast to \mathbf{b} (88) is often seen.

This results in the *spectral decomposition*

$$\mathbf{b} = \mathbf{v}^2 = \mu_1 \mathbf{n}_1 \otimes \mathbf{n}_1 + \mu_2 \mathbf{n}_2 \otimes \mathbf{n}_2 + \mu_3 \mathbf{n}_3 \otimes \mathbf{n}_3, \quad (91)$$

which allows us to compute the matrix logarithm operation on \mathbf{b} by

$$\log \mathbf{b} = \log(\mu_1) \mathbf{n}_1 \otimes \mathbf{n}_1 + \log(\mu_2) \mathbf{n}_2 \otimes \mathbf{n}_2 + \log(\mu_3) \mathbf{n}_3 \otimes \mathbf{n}_3. \quad (92)$$

The analytical derivation using MATLAB SYMBOLIC TOOLBOX [25] leads di-

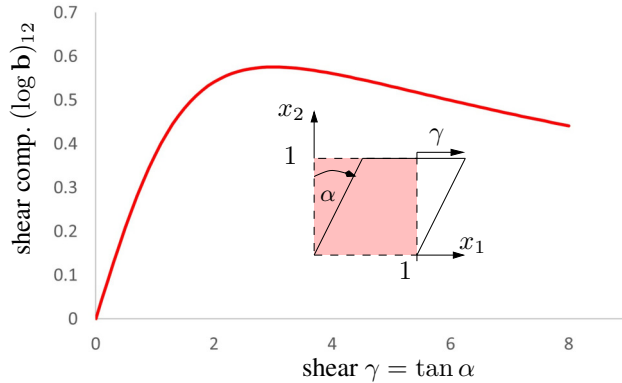


Figure 21: Shear component $(\log \mathbf{b})_{12}$ as function of shear measure $F_{12} = \gamma = \tan \alpha$, which in this context is no means a monotonous function.

rectly to the closed form expression

$$(\log \mathbf{b})_{12} = \frac{\log(\gamma \sqrt{\gamma^2 + 4} + \frac{\gamma^3}{2} \sqrt{\gamma^2 + 4} + 2\gamma^2 + \frac{\gamma^4}{2} + 1)}{\sqrt{\gamma^2 + 4}} \quad (93)$$

for the 12-shear component of (92) as function of the shear measure γ in (87). The graphical representation of (93) is given in Fig. 21 and shows a drop in the curve after $\gamma \simeq 3$, which indicates a non-monotonicity even in the log strain as function of the shear measure γ . Thus, HENCKY'S quadratic model $\sigma = \mu \log \mathbf{b}$ satisfies HILL's inequality, but predicts a non-monotone shear-stress curve $\tau_{12} = \mu (\log \mathbf{b})_{12}$.

References

- [1] ABAQUS: Theory Manual. Simulia, Providence, RI, USA (2009)
- [2] ABAQUS: Standard User's Manual. Simulia, Providence, RI, USA (2020)

- [3] Anssari-Benam, A., Goriely, A., Saccomandi, G.: Generalised invariants and pseudo-universal relationships for hyperelastic materials: A new approach to constitutive modelling. *J. Mech. Phys. Solids* **193** (2024). DOI <https://doi.org/10.1016/j.jmps.2024.105883>
- [4] ANSYS: Mechanical APDL Theory Manual. Ansys, Inc. (2025)
- [5] Baaser, H., Hopmann, C., Schobel, A.: Reformulation of strain invariants at incompressibility. *Archive Appl. Mech.* **83**(10.1007/s00419-012-0652-2), 273–280 (2013)
- [6] Blesgen, T., Holthausen, S., Husemann, N., Gmeineder, F., Neff, P.: Rate–form equilibrium for an isotropic Cauchy–elastic formulation. Part II: existence of weak solutions without rank–one convexity (2025). in preparation
- [7] Criscione, J., Humphrey, J., Douglas, A., Hunter, W.: An invariant basis for natural strain which yields orthogonal stress response terms in isotropic hyperelasticity. *J. Mech. Phys. Solids* **48**, 2445–2465 (2000)
- [8] Diani, J., Gilormini, P.: Combining the logarithmic strain and the full–network model for a better understanding of the hyperelastic behavior of rubber-like materials. *J. Mech. Phys. Solids* **53**, 2579–2596 (2005)
- [9] Drucker, D.: A definition of stable inelastic material. *J. Appl. Mech.* **26**(1), 101–106 (1959)
- [10] d'Agostino, M.V., Holthausen, S., Bernardini, D., Sky, A., Ghiba, I.D., Martin, R.J., Neff, P.: A constitutive condition for idealized isotropic Cauchy elasticity involving the logarithmic strain. *J. Elasticity* **157**(23), 1–44 (2025). DOI 10.1007/s10659-024-10097-2
- [11] Fontes, V., Leitão, A., Pereira, A.: **Hypersym**: An Educational MATLAB Code for Hyperelasticity. *Comp. Appl. in Eng. Education* **33**:(e70037) (2025)
- [12] Ghiba, I.D., Martin, R.J., Apetrii, M., Neff, P.: Constitutive properties for isotropic energies in ideal nonlinear elasticity for solid materials: numerical evidences for invertibility and monotonicity in different stress-strain pairs (2025). URL <https://arxiv.org/abs/2509.00126>. to appear in *Math. Mech. Solids*
- [13] Graban, K., Schweickert, E., Martin, R.J., Neff, P.: A commented translation of Hans Richter's early work “The isotropic law of elasticity”. *Math. Mech. Solids* **24**(8), 2649–2660 (2019). DOI 10.1177/1081286519847495
- [14] Hill, R.: A general theory of uniqueness and stability in elastic–plastic solids. *J. Mech. Phys. Solids* **6**, 236–249 (1958)
- [15] Hill, R.: On constitutive inequalities for simple materials – I. *J. Mech. Phys. Solids* **16**(4), 229–249 (1968). DOI 10.1016/0022-5096(68)90031-8

- [16] Hill, R.: Constitutive inequalities for isotropic elastic solids under finite strain. *J. Mech. Phys. Solids* **314**(1519), 457–472 (1970). DOI <https://doi.org/10.1098/rspa.1970.0018>
- [17] Holzapfel, G.: *Nonlinear Solid Mechanics*. Wiley (2000)
- [18] Horgan, C., Murphy, J.: Some remarks on the principal stretch versus invariant formulation for constitutive modeling of incompressible isotropic hyperelastic materials. *J. Elasticity* **157**(50) (2025). DOI <https://doi.org/10.1007/s10659-025-10142-8>
- [19] Hutter, K., Baaser, H. (eds.): *Deformation and Failure in Metallic Materials, Lecture Notes in Applied and Computational Mechanics*, vol. 10. Springer (2003)
- [20] Itskov, M.: *Tensor Algebra and Tensor Analysis for Engineers: With Applications to Continuum Mechanics*, 2 edn. ISBN 3540939067. Springer (2009)
- [21] Klein, D., Wollner, M., Baaser, H., Neff, P.: Enforcing polyconvexity and true-stress–true-strain monotonicity for incompressible isotropic hyperelasticity with neural network constitutive models (2025). In preparation
- [22] Korelc, J.: Automatic generation of finite-element code by simultaneous optimization of expressions. *Theoretical Computer Science* **187**(1-2), 231–248 (1997)
- [23] Kossa, A.: Closed-form analytical solutions for stability bounds of the incompressible Mooney–Rivlin hyperelastic model under standard homogeneous loadings. *International Journal of Applied Mechanics* **17**(03), 2550015 (2025). DOI 10.1142/S1758825125500152
- [24] Lee, E.: Elastic–plastic deformation at finite strains. *J. Applied Mechanics* **36**, 1–6 (1969)
- [25] MathWorks, T.M.I.: Matlab (R2024b) (2024). URL <https://www.mathworks.com>
- [26] Nedjar, B., Baaser, H., Martin, R.J., Neff, P.: A finite element implementation of the isotropic exponentiated Hencky–logarithmic model and simulation of the eversion of elastic tubes. *Computational Mechanics* **63**(4), 635–654 (2018). DOI: 10.1007/s00466-017-1518-9
- [27] Neff, P., Eidel, B., Martin, R.J.: Geometry of logarithmic strain measures in solid mechanics. *Archive for Rational Mechanics and Analysis* (2015). DOI DOI: 10.1007/s00205-016-1007-x
- [28] Neff, P., Ghiba, I.D., Lankeit, J.: The exponentiated Hencky–logarithmic strain energy. Part I: Constitutive issues and rank–one convexity. *J. Elasticity* **121**(2), 143–234 (2015)

[29] Neff, P., Holthausen, S., d'Agostino, M., Bernardini, D., Sky, A., Ghiba, I., Martin, R.J.: Hypo-elasticity, Cauchy-elasticity, corotational stability and monotonicity in the logarithmic strain. *J. Mech. Phys. Solids* **202** (2025). DOI <https://doi.org/10.1016/j.jmps.2025.106074>

[30] Neff, P., Husemann, N., A.S. Nguetcho Tchakoutio, S.K., Martin, R.J.: The corotational stability postulate: Positive incremental Cauchy stress moduli for diagonal, homogeneous deformations in isotropic nonlinear elasticity. *Int. J. Non-Linear Mech.* **174**(105033) (2025). DOI [10.1016/j.ijnonlinmec.2025.105033](https://doi.org/10.1016/j.ijnonlinmec.2025.105033)

[31] Neff, P., Husemann, N., Holthausen, S., Gmeineder, F., Blesgen, T.: Rate-form equilibrium for an isotropic Cauchy-elastic formulation. Part I: Modeling. *arXiv* (2504.11327) (2025). to appear in *J. Nonlinear Sci.*

[32] Neff, P., Lankeit, J., Madeo, A.: On Grioli's minimum property and its relation to Cauchy's polar decomposition. *International Journal of Engineering Science* **80**, 209–217 (2014). DOI <https://doi.org/10.1016/j.ijengsci.2014.02.026>. URL <https://www.sciencedirect.com/science/article/pii/S0020722514000470>

[33] Ogden, R.: Large deformation isotropic elasticity - on the correlation of theory and experiment for incompressible rubberlike solids. *Proc. R. Soc. Lond. A* **326**, 565—584 (1972)

[34] Richter, H.: Das isotrope Elastizitätsgesetz. *Z. angew. Math. Mech.* **28**(7–8), 205–209 (1948). DOI [10.1002/zamm.19480280703](https://doi.org/10.1002/zamm.19480280703)

[35] Richter, H.: Hauptaufsätze: Verzerrungstensor, Verzerrungsdeviator und Spannungstensor bei endlichen Formänderungen. *Z. angew. Math. Mech.* **29**(3), 65–76 (1949). DOI <https://doi.org/10.1002/zamm.19490290301>

[36] Rivlin, R., Saunders, D.: Large elastic deformations of isotropic materials. Experiments on the deformation of rubber. *Philosophical Transactions of the Royal Society of London. Series A, Mathematical and Physical Sciences* **243**, 251–288 (1952)

[37] Schneider, K., Calabrò, R., Lombardi, R., Kipscholl, C., Horst, T., Schulze, A., Dedova, S., Heinrich, G.: Characterisation of the Deformation and Fracture Behaviour of Elastomers Under Biaxial Deformation, pp. 335–349. Springer International Publishing, Cham (2017)

[38] Sidoroff, F.: Sur les restrictions à imposer à l'énergie de déformation d'un matériau hyperélastique. *Comptes Rendus de l'Académie des Sciences* **279**, 379–382 (1974)

[39] Treloar, L.: The Physics of Rubber Elasticity, 3th edn. ISBN 0198570279. Oxford University Press (1975)

[40] Wolfram, W.R.I.: Mathematica, Version 14.2. Champaign, IL, 2024

- [41] Wollner, M., Holzapfel, G., , Neff, P.: In search for constitutive conditions in isotropic hyperelasticity: polyconvexity versus true-stress–true-strain monotonicity. arXiv (2509.08597v1) (2025). to appear in *J. Mech. Phys. Solids*
- [42] Wriggers, P.: Nonlinear Finite Element Methods. Springer (2008)
- [43] Yao, Y., Chen, S., Huang, Z.: A generalized Ogden model for the compressibility of rubber-like solids. *Phil. Trans. R. Soc. A* **380**: 20210320 (2022). DOI <https://doi.org/10.1098/rsta.2021.0320>
- [44] Yeoh, O.: Some forms of the strain energy function for rubber. *Rubber Chemistry and Technology* **66**(5), 754–771 (1993). DOI 10.5254/1.3538343